

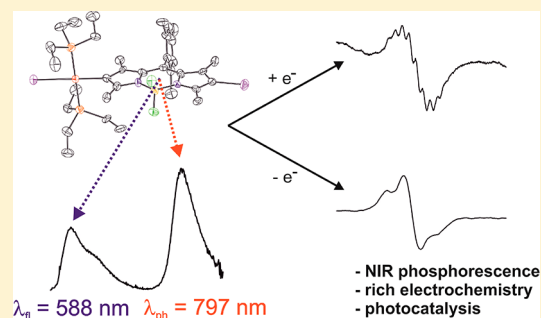
σ -Pt-BODIPY Complexes with Platinum Attachment to Carbon Atoms C2 or C3: Spectroscopic, Structural, and (Spectro)Electrochemical Studies and Photocatalysis

Peter Irmeler and Rainer F. Winter*[✉]

Fachbereich Chemie, Universität Konstanz, Universitätsstraße 10, D-78457 Konstanz, Germany

S Supporting Information

ABSTRACT: In this work we discuss five new complexes with the general formula *trans*-Pt(bodipy)I(PET₃)₂, where differently substituted bodipy dyes attach to the coordination center via a direct Pt–C σ -bond to the pyrrolic carbon atom C2 or C3. We also report an isolable intermediate of the oxidative addition step where the bodipy is η^2 -bonded to the *cis*-Pt(0)(PET₃)₂ moiety. Comparison between the new complexes, *meso*-platinated analogue **8-Pt**, and the parent dyes reveals that the site of platinum attachment influences the spectroscopic, photophysical, electrochemical, and electronic properties. In contrast to **8-Pt**, absorption and emission bands are red-shifted with respect to the parent dyes. 2-Platinated bodipy dyes **2-Pt-6H**, **2-Pt-6I**, **2-Pt-Mes-6I**, and **2-Pt-6Et** exhibit dual fluorescence and NIR phosphorescence emissions, with low quantum yields, whereas **3-Pt** emits solely by fluorescence ($\Phi_{\text{Fl}} = 52.7\%$). The complexes are modestly efficient sensitizers for photochemical ¹O₂ production but outperform methylene blue. They also undergo one reversible one-electron reduction and oxidation as indicated by cyclic voltammetry. Half-wave potentials are cathodically shifted by 340–510 mV with respect to the parent dyes. The one-electron reduced and some of the one-electron oxidized forms were generated and investigated by UV/vis/NIR and EPR spectroscopy as well as TD-DFT calculations. The similarity of their spectra to those of the one-electron reduced or oxidized forms of other bodipy dyes as well as the richly structured EPR spectra and *g*-values close to *g*_e attest to a dominant bodipy character of the relevant frontier MOs.



INTRODUCTION

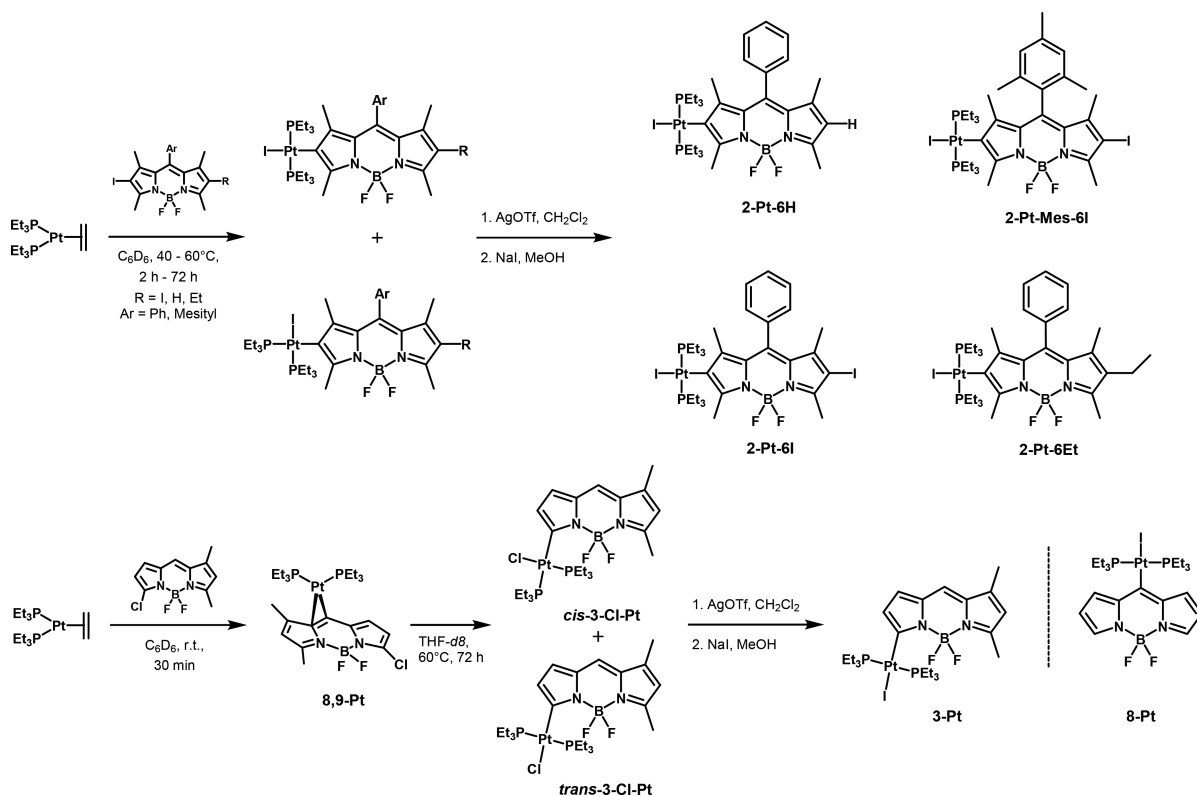
Color has always fascinated mankind. The fabrication of dyes has been key to the development of synthetic organic chemistry and the shaping of modern chemical industry. Nowadays, myriads of dyes allow for generating any desired hue of color. More recently, dyes have gained importance as sensitizers in organic or organometallic light-emitting diodes (OLEDs)^{1,2} or for bioimaging purposes.^{3,4} Further applications of modern dyes rely on their capability to undergo efficient intersystem crossing (ISC) to their excited triplet states T₁ and to radiatively relax to the electronic ground S₀ state by phosphorescence emission. The significantly longer phosphorescence lifetime (usually by three or more orders of magnitude) compared to fluorescence from the excited singlet state S₁ opens further avenues for such photosensitizers like their utilization in dye-sensitized solar cells (DSSCs),⁵ photocatalysis,^{6–8} photodynamic therapy,^{9–12} or triplet–triplet annihilation (TTA) upconversion.^{13,14}

The family of 4,4-difluoro-4-bora-3a,4a-diaza-s-indacene-8-yl (bodipy) fluorophores holds a particularly prominent place in these respects. Their chemical robustness and easy derivatization allow for precise adjustment of the energy levels of the excited singlet and triplet states of bodipy dyes, to decorate bodipys with a huge variety of substituents, and to incorporate them into a vast number of functional arrays.^{15–18} This endows

them with the capabilities of energy or charge transfer between their individual constituents on photoexcitation^{2,19–21} or makes them amenable to bioconjugate chemistry for medical purposes.^{22–24} Effective ISC to the excited triplet state of bodipys has been known since 2005,²⁵ when it was observed that the fluorescence quantum yield (QY) of 2,6-diiodo-bodipy is strongly reduced with respect to the nonhalogenated dye due to the competitiveness of ISC with fluorescence emission. Further progress was made by linking two bodipys to rigid orthogonal arrays^{26–30} or bringing bodipy dyes into the coordination sphere of a heavy metal ion such as ruthenium, rhodium, iridium, or platinum, usually by covalently attaching them to a polypyridine ligand motif or by introducing them as acetylide ligands.^{31–40} Representative examples of the latter kind of compounds are mono- and dinuclear Pt(II) bipyridine or diphosphane bis(acetylide) complexes with two identical or nonidentical bodipy-acetylide ligands.^{32–35,40} Most of these complexes exhibit dual fluorescence and phosphorescence emissions with, however, usually rather modest phosphorescence QYs at room temperature (r.t.). Upon lowering the temperature or embedding the compounds into solid films, the phosphorescence QY may be significantly increased.^{32,34,41}

Received: November 6, 2017

Scheme 1. Overview of the Complexes and Their Syntheses



Experimental and quantum chemical studies show that the frontier molecular orbitals (FMOs) of the latter platinum complexes are dominated by the acetylide ligands with only modest contributions from the platinum ion(s). The platinum ion then acts as a remote heavy atom. In this scenario, the efficacy of ISC scales with d^{-6} and therefore rapidly decreases with increasing spatial separation d of the center of the π chromophore from the heavy metal ion.^{42–44} It is therefore advantageous to bring the platinum ion as close to the chromophore as possible, in particular by attaching the dye to the heavy metal ion via a direct metal–carbon σ -bond. That approach was first applied to anthracenes,⁴⁵ perylenes,⁴⁶ corannulenes,^{47,48} or dibenz[*a,c*]anthracenes.⁴⁹ The latter chromophores were introduced into the coordination sphere of a platinum ion via oxidative addition of the corresponding haloarene to a bis(phosphane) platinum(0) source such as $\text{Pt}(\text{PR}_3)_4$ or $\text{Pt}(\text{PR}_3)_2(\eta^2\text{-olefin})$. The resulting σ -aryl Pt(II) complexes, however, were mostly only fluorescent, again as a result of the large distance between the heavy metal ion and the center of the extended π -chromophore.

We have recently observed that platinum complexes *cis/trans*- $\text{Pt}(\text{PR}_3)_2\text{X}$ (R = Ph, Et; X = monoanionic ligand) with a σ -bonded thioxanthonyl or bodipy ligand show dual fluorescence and phosphorescence emissions with phosphorescence QYs of up to 41% in fluid solution at r.t., even though the free ligands are not or only very weakly phosphorescent under these conditions. So far these studies only involved complexes where the platinum ion attaches to the bodipy dye via its *meso* position C8. As an expansion of our previous work, we here report on five new complexes where the metal ion binds to the pyrrolic carbon atoms C2 or C3 of a bodipy dye (see Scheme 1). Monoplatination of diiodo-derivatives of the bodipys also allows us to compare analogous complexes with or

without additional iodo atoms at the bodipy dye and to probe for the additional heavy atom effect of the remaining iodo substituent.

In this context one should note that the HOMO of bodipys has a nodal plane along the B–C8 vector.^{50,51} This severely limits platinum contribution to the HOMO, thus reducing the impact of the $\text{Pt}(\text{PR}_3)_2\text{X}$ fragment to that of a potent electron donor with a remote heavy atom. In contrast, positions C2 and C3 have large contributions to the FMOs. Platinum attachment to any of these positions is therefore expected to cause major perturbations of the bodipy π -system which should become manifest in their optical, photophysical, and electrochemical properties.^{8,33,41,52–56} Quantum chemical calculations have also been performed and are augmented by UV/vis/NIR and EPR spectroelectrochemical studies to directly probe for the identity of the respective redox sites and the platinum contribution to the SOMO of the reduced and oxidized forms of these complexes.

RESULTS AND DISCUSSION

Synthesis and Characterization. All new complexes of this study and their syntheses are summarized in Scheme 1. The platinum fragment was introduced by oxidative addition of the corresponding 2- or 3-halogenated bodipy dye to $\text{Pt}(\eta^2\text{-C}_2\text{H}_4)(\text{PEt}_3)_2$, which itself is conveniently prepared from the diethyl complex by thermally induced reductive elimination of ethane.⁵⁷ Those reactions inevitably afforded mixtures of the *cis* and *trans* isomers, which were conveniently converted to the pure *trans* complexes by successive treatment with AgOTf and NaI. Quite interestingly, further reaction of complexes 2-Pt-Mes-6I and 2-Pt-6I with an additional equivalent of $\text{Pt}(\eta^2\text{-C}_2\text{H}_4)(\text{PEt}_3)_2$ or direct treatment of the 2,6-diiodinated dye with 2 equiv of the platinum precursor failed in our hands to

Table 1. Selected Bond Lengths [Å] and Angles [deg] for the Complexes

bond parameter	2-Pt-6H ^a	2-Pt-6I	2-Pt-Mes-6I	2-Pt-6Et ^a	3-Pt
Pt–C _{bodipy}	2.027(4) 2.023(4)	2.018(4)	1.991(11)	2.016(7) 2.020(7)	1.977(7)
Pt1–I	2.6943(4) 2.6872(4)	2.6852(3)	2.6812(9)	2.6766(6) 2.6841(7)	2.6849(5)
Pt1–P1	2.3119(14) 2.3022(14)	2.2992(11)	2.299(3)	2.305(2) 2.301(2)	2.326(2)
Pt1–P2	2.3142(14) 2.3064(15)	2.3181(10)	2.304(4)	2.306(2) 2.303(2)	2.325(2)
C8–C9	1.404(7) 1.393(7)	1.427(5)	1.425(17)	1.421(11) 1.400(11)	1.392(11)
C–Pt1–P1	89.73(14) 90.56(15)	92.82(11)	90.3(4)	90.6(3) 90.1(2)	89.7(3)
C–Pt1–P2	91.46(14) 91.10(15)	88.16(11)	90.2(4)	91.4(3) 89.6(2)	90.6(3)
I1–Pt1–P1	89.37(3) 89.20(3)	88.77(3)	90.56(9)	89.28(5) 90.08(6)	91.24(7)
I1–Pt1–P2	89.48(3) 89.22(4)	90.27(3)	88.95(8)	89.45(6) 90.24(5)	89.29(7)
P1–Pt1–P2	178.48(5) 176.02(5)	177.31(3)	177.15(16)	172.68(8) 178.56(9)	175.18(9)
C–Pt1–I1	177.11(15) 178.63(14)	178.38(10)	177.30(11)	174.4(2) 179.2(3)	170.0(2)
[B]–[Pt] ^b	85.7 85.5	85.4	88.28	88.8 88.5	89.6
[B]–[Ar] ^c	76.9 83.7	80.3	86.86	79.8 88.9	
[Pyr]–[Pyr] ^d	5.2 3.2	3.4	7.0	2.0 6.4	6.5

^aData for the two independent molecules of the unit cell. ^bInterplanar angle between the best plane through the inner six-membered ring of the bodipy ligand and the coordination plane at the platinum ion. ^cInterplanar angle between the best plane through the inner six-membered ring of the bodipy ligand and the *meso*-aryl substituent. ^dInterplanar angle between the two pyrrolic subunits of the bodipy ligand.

provide the dinuclear complexes, even under forcing conditions. This is possibly due to electronic deactivation on the introduction of the first platinum fragment. The stronger C–Cl bond of the 3-chloro-5,7-dimethylbodipy increases the energy barrier for oxidative addition such that the intermediate substitution product **8,9-Pt**, where the ethylene ligand of the precursor is replaced by the η^2 -coordinated bodipy, can be isolated. Owing to the poor solubility of that complex in benzene, crystals suitable for X-ray molecular structure determination were directly deposited from the reaction solution. Above 40 °C in THF-*d*₆, **8,9-Pt** slowly converts to the products of oxidative addition. Full conversion required 72 h at 60 °C as depicted in Figure S1 and afforded a mixture of *trans*- and *cis*-**3-Cl-Pt** with the *cis* isomer as the kinetic and the *trans* isomer as the thermodynamically preferred product. Van der Boom and co-workers have reported on a similar intermediate with η^2 -coordination of a d¹⁰ Pt(0) center to the C=C double bond of a brominated stilbazole. After primary coordination to a remote double bond, the low valent platinum center migrates along the conjugated π -system until it reaches the halogenated double bond.⁵⁸

All complexes were readily identified by multinuclear (¹H, ¹³C, ³¹P, and ¹⁹⁵Pt) NMR spectroscopy and their purities confirmed (see Figures S2–S30). The ³¹P NMR spectra of the *trans*-Pt(bodipy)I(PEt₃)₂ complexes feature just one sharp singlet which is located at 7.69 ppm for **3-Pt** or in between 9.03 and 9.75 ppm for the 2-platinated bodipy complexes and is symmetrically flanked by ¹⁹⁵Pt satellites ($J_{\text{PtP}} = 2540\text{--}2560$

Hz). The ¹⁹⁵Pt NMR resonance signal of every complex is consequently split into a triplet with a chemical shift of –4784 to –4802 ppm for the complexes where platinum(II) ion is bound to C2 and of –4599 ppm for complex **3-Pt**. The presence of a direct Pt–C σ -bond was also confirmed by platinum satellites of the corresponding adjacent nuclei in the ¹H and ¹³C NMR spectra of the complexes. Owing to the orthogonal arrangement of the platinum coordination plane to the bodipy ligand (*vide infra*) and a hindered rotation around the Pt–C axis the methylene protons of the PEt₃ ligands are diastereotopic. For complexes with the platinum ion attached to carbon atom C2, shift differences are rather minor such that only slight broadening of the respective resonance signals is observed. **3-Pt**, however, shows two separate resonances for the methylene protons in its ¹H NMR spectrum (Figure S27).

Platinum coordination to the C8=C9 double bond of 3-chloro-5,7-dimethylbodipy in the complex **8,9-Pt** splits the resonance signal for H8 into a doublet of doublets with ³J_{PtH} couplings of 9.1 and 4.3 Hz to the two inequivalent phosphane ligands and additional platinum satellites with a ²J_{PtH} coupling constant of 49.2 Hz. As the result of η^2 -coordination, all corresponding resonance signals appear at higher field as compared to the parent dye. This is most dramatically seen for H8 and C8, whose resonances are shifted from 6.15 to 3.83 ppm (compare Figures S21 and S23) or from 123.5 to 42.1 ppm (compare Figures S22 and S26, $J_{\text{PtC}} = 43.6$ Hz). The ¹⁹⁵Pt NMR spectrum of **8,9-Pt** shows the expected doublet of doublets at $\delta = -4950$ ppm; the coupling constants J_{PtP} of 4800

and 3320 Hz match with the ^{195}Pt satellites in the ^{31}P NMR spectrum.

Single-Crystal X-ray Diffraction Analysis. Single crystals of complexes **2-Pt-6H**, **2-Pt-6I**, **2-Pt-Mes-6I**, and **2-Pt-6Et** as well as of complexes **3-Pt** and **8,9-Pt** were grown by the procedures given in the Experimental Section and were successfully subjected to X-ray diffraction analyses. Details of the data collection and structure refinement are collected in Table S1. The most important metric parameters derived from the structure solutions are provided in Tables 1 and 2. The unit

Table 2. Selected Bond Lengths [Å] and Angles [deg] for 8,9-Pt

bond parameters	8,9-Pt
C8–Pt1	2.127(9)
C9–Pt1	2.226(9)
Pt1–P1	2.301(2)
Pt1–P2	2.229(3)
C8–C9	1.431(13)
C8–Pt1–C9	38.3(4)
C8–Pt1–P2	97.5(3)
C9–Pt1–P1	120.0(3)
C8–Pt1–P1	157.9(3)
C9–Pt1–P2	135.8(3)
P1–Pt–P2	103.92(9)
[B]–[Pt] ^a	81.6
[Pyr]–[Pyr] ^b	17.0

^aInterplanar angle between the best plane through the inner six-membered ring of the bodipy ligand and the coordination plane at the platinum ion. ^bInterplanar angle between the planes of the pyrrolic subunits.

cell of **8,9-Pt** contains both different enantiomers that result from platinum coordination to either the Re or Si face of the prochiral olefin. The crystal of **2-Pt-6I** contained highly disordered molecules of *n*-pentane. All attempts to refine the solvent molecules were unsuccessful and the corresponding reflexes were removed using the solvent mask tool in OLEX2.

The molecular structures are displayed in Figure 1. Every σ -bodipy platinum complex exhibits an almost ideal square-planar coordination geometry at the coordination center with the *cis* bond angles at the platinum ion close to 90°. The P–Pt–P angle is slightly bent at 172.68–178.56°. The coordination plane at the platinum atom as defined by the atoms Pt, P1, P2, I, and C2 or C3 is in a close to orthogonal orientation (interplanar angles 85.4–89.6°) with respect to the plane through the inner six-membered ring of the attached bodipy ligand. The lengths of the Pt–C2 σ -bonds fall within a narrow range of 1.991(11)–2.027(4) Å and are nearly identical within the limits of the standard deviations, while the bond length Pt–C3 of 1.977(7) Å is slightly shorter. Previously reported **8-Pt**, where the Pt ion attaches to the *meso* position of the bodipy, has a similar Pt–C bond length of 1.994(10) Å.⁵⁹ With interplanar angles of 76.9–88.9°, the *meso* aryl substituents are also in a close to orthogonal orientation with the bodipy plane. The C8–Pt–C9 bond angle of 38.3(4)° and the angle P1–Pt–P2 of 103.92(9)° (Table 2) closely resemble those of other diphosphane platinum olefin complexes in the literature.^{58,60,61} The Pt–C bond lengths are longer than those of 2.031(3)–2.114(4) Å found for related compounds, while the

C–C bond length of 1.431(13) Å is still in the usual range of 1.275(3)–1.454(6) Å.^{58,60,61}

Not unexpectedly, the Pt–C bond to the sterically less hindered carbon atom C8 of 2.127(9) Å is significantly shorter than that of 2.226(9) Å to the pyrrolic carbon atom C9. The coordination plane at the platinum atom as defined by the atoms Pt, P1, P2, C8, and C9 forms an interplanar angle of 81.5° with the plane of the bodipy ligand. η^2 -Coordination to the C8=C9 bond and concomitant rehybridization of the *meso* carbon atom causes a larger deviation of the pyrrole rings from coplanarity of 17.0° (Table 2) as compared to that of 2.0–7.0° for the other complexes (Table 1). The distortion nevertheless remains small and is thus not expected to severely impact on π -conjugation within the bodipy ligand.

Packing diagrams of the various crystal structures are provided as Figures S31–S36. Short intermolecular H···I contacts between pyrrolic (**3-Pt**, **2-Pt-6H**) or the *meso* H atom (**3-Pt**, $d(\text{H}\cdots\text{I}) = 3.005$ Å) and the iodide ligand as well as short intermolecular H···F contacts between the BF₂ group and methyl (**8,9-Pt**, $d(\text{H}\cdots\text{F}) = 2.612$ Å) and/or methylene protons of the PEt₃ ligands (**8,9-Pt**, $d(\text{H}\cdots\text{F}) = 2.579$ Å; **2-Pt-6I**, $d(\text{H}\cdots\text{F}) = 2.561$ Å, **2-Pt-6H**, and $d(\text{H}\cdots\text{F}) = 2.490$ Å) or to cocrystallized benzene (**2-Pt-6I**, $d(\text{H}\cdots\text{F}) = 2.537$, 2.571, and 2.658 Å) or CH₂Cl₂ molecules (**2-Pt-6Et**, $d(\text{H}\cdots\text{F}) = 2.480$ Å) are found.

Electronic Absorption Spectroscopy. Figures 2 and S37 display the electronic absorption spectra of the parent dyes and their platinum complexes, while Table 3 lists all relevant data including band assignments and calculated transition energies derived from time-dependent density functional theory (TD-DFT; for comparisons of experimental and calculated spectra see Figures S38–S40). Remarkably, η^2 -coordination of the 3-chloro-5,7-dimethylbodipy dye to the Pt(PEt₃)₂ moiety does not affect the position and intensity of the characteristic bodipy $\pi \rightarrow \pi^*$ band. Complex **8,9-Pt** and the parent dye have their absorption maximum at 508 nm, and, on platinum coordination, the extinction coefficient is reduced by about the same factor as the molecular mass increases. Geometry optimization of the molecular structure on the pbe1pbe/6-31g(d) level with the CH₂Cl₂ solvent accounted for by the PCM formalism overestimates the structural perturbation due to η^2 -coordination somewhat. Thus, the two pyrrole rings are more bent with a calculated interplanar angle of 24.5° as opposed to the experimental value of 17.0° (*vide supra*). The calculated stronger structural distortion might also cause some differences between the TD-DFT calculated and experimental spectra in terms of the energetic ordering of the individual transitions as indicated by Figure S40.

According to our calculations all relevant MOs of **8,9-Pt** receive strong contributions from the Pt(PEt₃)₂ fragment (40 and 37%, respectively as inferred from Mulliken decomposition analysis, see Table S2). An intense absorption arising from the typical $\pi \rightarrow \pi^*$ excitation of the π -coordinated bodipy dye is calculated as the HOMO–1 \rightarrow LUMO transition and hence at higher energy than the weaker, but still rather strong, HOMO \rightarrow LUMO band (see Figure S41). The latter transition is predicted to have appreciable intraligand charge-transfer (CT) character with a shifting of electron density from the chloro-substituted to the dimethyl-substituted pyrrole ring. Both, the relative intensities and the solvatochromism of these bands rather point to an opposite ordering of the HOMO and HOMO–1 levels. Thus, the prominent band at ca. 500 nm is only slightly solvatochromic with a blue shift of 280 cm^{–1}

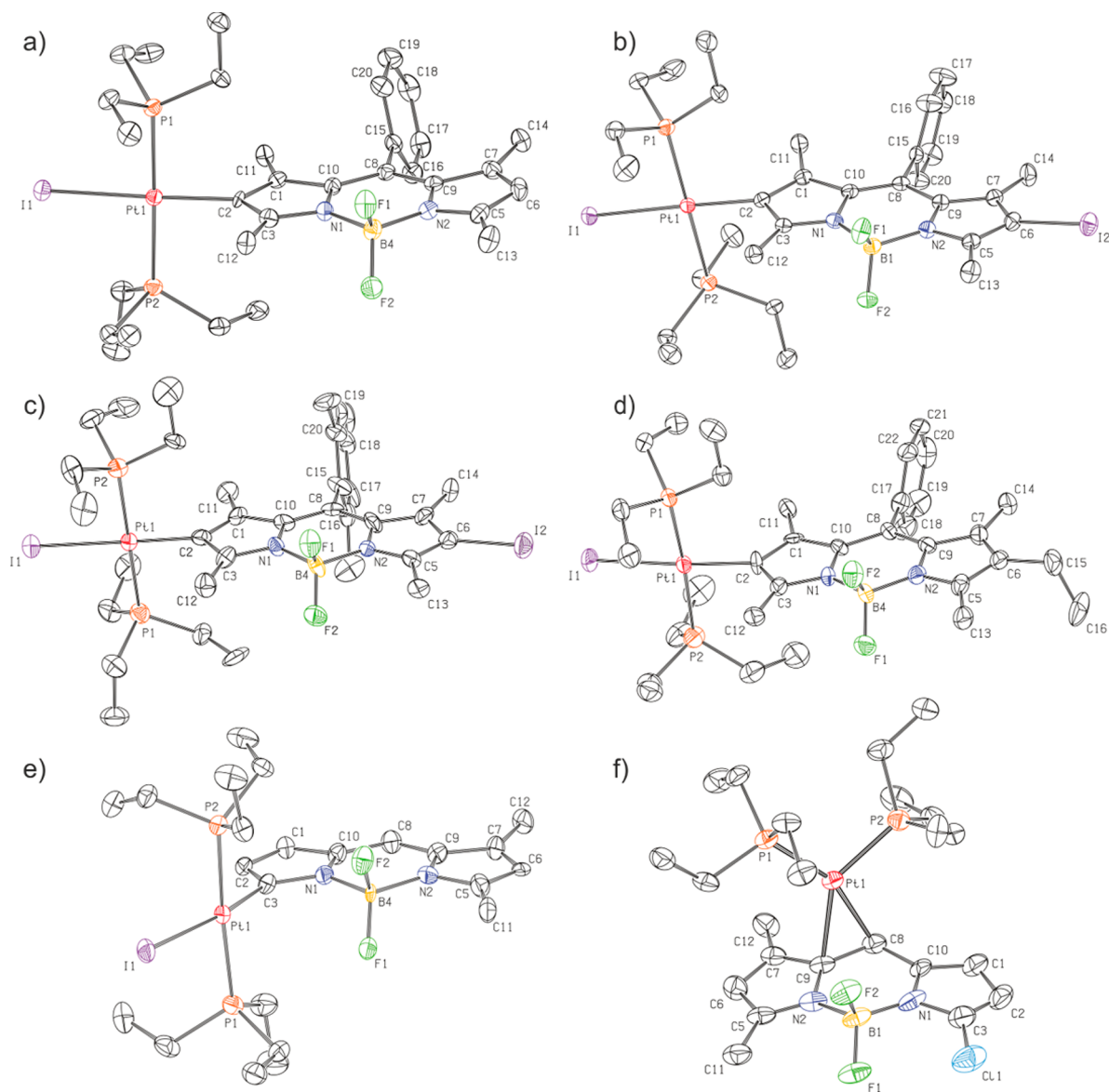


Figure 1. ORTEP⁶² diagrams of (a) 2-Pt-6H, (b) 2-Pt-6I, (c) 2-Pt-Mes-6I, (d) 2-Pt-6Et, (e) 3-Pt, and (f) 8,9-Pt. The ellipsoids are drawn at a 50% probability level. Solvent molecules and hydrogen atoms are omitted for reasons of clarity. For 2-Pt-6H, 2-Pt-6Et, and 8,9-Pt only one of the two independent molecules of the unit cell are shown.

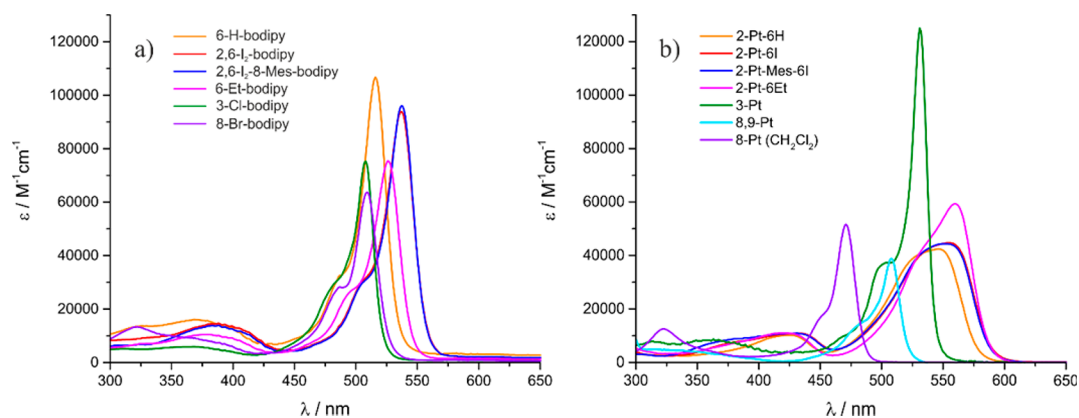


Figure 2. (a) Electronic absorption spectra of the halogenated dye precursors in ca. 1×10^{-5} M toluene solutions. (b) UV-vis spectra of the bodypy platinum complexes in ca. 1×10^{-5} M toluene solutions.

Table 3. Absorption Data of the Complexes in ca. 1×10^{-5} M Solutions in THF, Toluene, or CH_2Cl_2 and TD-DFT-Calculated (PBE1PBE/6-31G(d) PCM (CH_2Cl_2)) Energies and Band Assignments^a

compound	solvent	absorption data		TD-DFT calculations			
		$\lambda_{\text{max}}/\text{nm}$ ($\epsilon/\text{L mol}^{-1} \text{cm}^{-1}$)		λ (nm)	f^{c}	major contributions	Assignment
2-Pt-6H	toluene	324 (3100), 399 (7500), 425 (10300), 532 (40700), 546 (42400)				n.c. ^b	
	CH_2Cl_2	321 (4200), 400 (8000), 425 (10700), 531 (36100)					
	THF	321 (4500), 400 (8200), 424 (10700), 537 (39300)					
2-Pt-6I	toluene	393 (7600), 433 (11000), 534 (41200), 554 (44700)				n.c. ^b	
	CH_2Cl_2	393 (7600), 433 (11000), 535 (36000), 552 (35900)					
	THF	393 (7600), 431 (11100), 535 (36000), 555 (34200)					
2-Pt-Mes-6I	toluene	362 (7300), 384 (8900), 430 (10900), 530 (38300), 553 (44400)		465	0.66	HOMO \rightarrow LUMO (94%)	$\pi \rightarrow \pi^*$
				392	0.26	HOMO-3 \rightarrow LUMO (23%), HOMO-1 \rightarrow LUMO (70%)	ML \rightarrow L'CT ^a
	CH_2Cl_2	381 (7400), 418 (10700), 430 (11300), 528 (38800), 553 (40900)		352	0.032	HOMO-5 \rightarrow LUMO (76%), HOMO-3 \rightarrow LUMO (11%)	ML \rightarrow L'CT, ^a ILCT ^a
	THF	378 (6200), 415 (8600), 430 (9110), 529 (39300), 554 (40800)		335	0.083	HOMO-7 \rightarrow LUMO (97%)	ILCT ^a
				261	0.082	HOMO-13 \rightarrow LUMO (91%)	ML \rightarrow L'CT ^a
2-Pt-6Et	toluene	377 (6900), 420 (11000), 541 (47400), 560 (59300)				n.c. ^b	
	CH_2Cl_2	378 (8000), 420 (11600), 535 (40700), 556 (49000)					
	THF	384 (7700), 421 (10700), 539 (44000), 556 (51500)					
8,9-Pt	toluene	320 (4800), 508 (38900)		409	0.19	HOMO \rightarrow LUMO (96%)	ILCT ^a with mc ^c
	THF	349 (4800), 501 (37900)		334	0.36	HOMO-1 \rightarrow LUMO (86%)	$\pi \rightarrow \pi^*$ with mc ^c
3-Pt	toluene	314 (7900), 359 (8300), 531 (125000)		439	0.77	HOMO \rightarrow LUMO (99%)	$\pi \rightarrow \pi^*$
	CH_2Cl_2	312 (4400), 355 (4400), 528 (101100)		334	0.070	HOMO-4 \rightarrow LUMO (97%)	ILCT ^a
	THF	312 (4400), 355 (4400), 527 (109300)		248	0.064	HOMO-10 \rightarrow LUMO (91%)	ML \rightarrow L'CT ^a
8-Pt	CH_2Cl_2	323 (12500), 344 (6500), 471 (51600)		392	0.39	HOMO \rightarrow LUMO (97%)	$\pi \rightarrow \pi^*$
				309	0.07	HOMO-5 \rightarrow LUMO (81%)	ML \rightarrow L'CT ^a
				295	0.17	HOMO-6 \rightarrow LUMO (90%)	$\pi \rightarrow \pi^*$

^a f = Oscillator strength, ML \rightarrow L'CT = metal/ligand to ligand' charge transfer, ILCT = intraligand charge transfer. ^bNot calculated. ^cmc = Metal contribution.

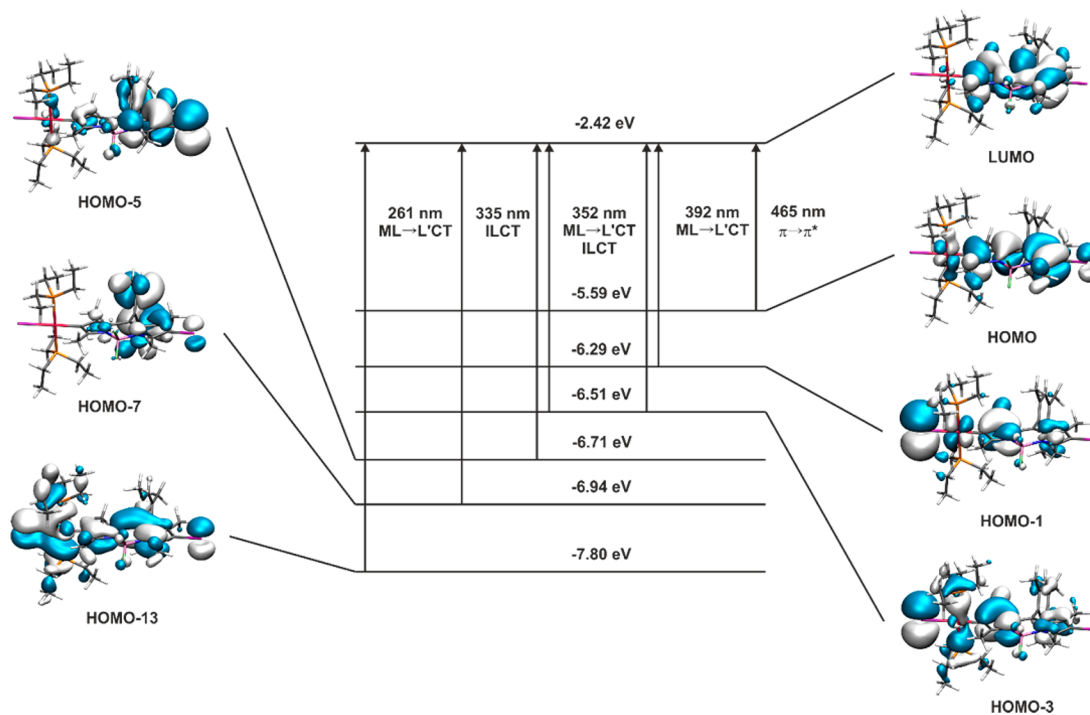


Figure 3. Graphical representation of the relevant MOs, transitions, and TD-DFT energies of 2-Pt-Mes-6I. Solid arrows symbolize the main contributor(s) to the respective transition.

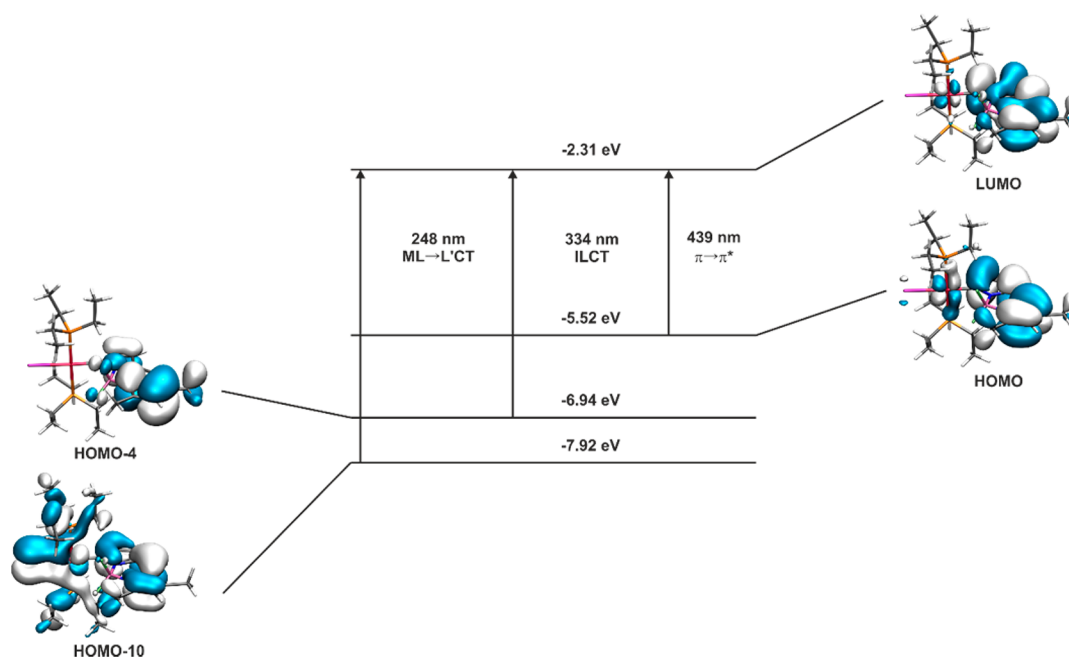


Figure 4. Graphical representation of the relevant MOs, transitions, and TD-DFT energies of 3-Pt. Solid arrows symbolize the main contributor to the respective transition.

Table 4. Photophysical Data of the σ -Bodipy Platinum Complexes in Degassed CH_2Cl_2 , Toluene, or 2-Me-THF Solutions at Concentrations of ca. 10^{-6} M at r. t.

	$\lambda_{\text{max,Fl}}/\text{nm}$ (Stokes shift/ cm^{-1})	$\lambda_{\text{max,Ph}}/\text{nm}$ (Stokes shift/ cm^{-1})	Φ_{Fl}	Φ_{Ph}	Φ_{Δ}^c	τ_{Fl} (ns)	τ_{Ph} (μs)	$k_{\text{ISC,S}_1\rightarrow\text{T}_1}^j$ (s^{-1})	$k_{\text{ISC,T}_1\rightarrow\text{S}_0}^j$ (s^{-1})
8-Pt	481 (441)	637 (5669) ^a	0.002	0.364 ^a	0.95	0.484	297 ± 2^a	2.1×10^9	2.0×10^3
2-Pt-6H	580 (1074)	804 (5877)	0.0008 ^b	0.0009 ^b	0.51	4.5 ± 0.2	$80 \pm 4,$ $765 \pm 8,$ 475 ± 9^d	2.2×10^8	1.3×10^4
2-Pt-6I	590 (1036)	804 (5548)	0.0003 ^b	0.0004 ^b	0.53	$3.7 \pm 0.2,$ ^d 30 ± 1^d	$67 \pm 3,$ $433 \pm 11,$ 247 ± 5^d		1.5×10^4
2-Pt-Mes-6I	588 (1109)	797 (5569)	0.0009 ^b	0.0014 ^b	0.48	n.d. ^e	$150 \pm 10,$ $843 \pm 64,$ 269 ± 9^d		6.7×10^3
2-Pt-6Et	587 (853)	815 (5619)	0.0006 ^b	0.0003 ^b	0.34	$4.12 \pm 0.09,$ $0.0459 \pm 0.008,$ 4.23 ± 0.09^d	$243 \pm 4,$ 683 ± 18^d	2.4×10^8	4.1×10^3
8,9-Pt	516 (305)		0.486		n.d. ^e	$5.33 \pm 0.02,$ 6.28 ± 0.04^g		0.96×10^8	
3-Pt	535 (141)		0.527		0.19	$2.30 \pm 0.01,$ 2.52 ± 0.01^d		2.06×10^8	
3-Cl-5,7-Me ₂ -bodipy ^h	501 (532)		0.73			5.60 ± 0.01			

^aMeasured in CH_2Cl_2 solution at r.t. ^bDetermined using 2,6-I₂-8-Ph-Bodipy ($\Phi = 3.13\%$) as a standard. ^c¹O₂ generation quantum yield corrected using the value of methylene blue (MB, $\Phi_{\Delta} = 0.57$) as a reference. ^dMeasured in 2-Me-THF glass at 77 K. ^eNot determined. ^f k_{ISC} is the rate constant for intersystem crossing and was estimated from eq 2. ^gMeasured in toluene glass at 77 K. ^hAccording to ref 64.

between toluene and THF, while the second, less intense band exhibits a sizable red shift of 2600 cm^{-1} , indicating a more polar excited state (see Figure S37f).

All complexes exhibit the characteristic sharp and intense $\pi \rightarrow \pi^*$ absorption band of a bodipy dye. Platinum coordination to the 2- or 3-position shifts the main absorption band bathochromic, e.g., from 508 nm for 3-chloro-5,7-dimethylbodipy to 531 nm ($\Delta\bar{\nu} = 850 \text{ cm}^{-1}$) for 3-Pt or from 516 nm for 2-iodo-8-phenylbodipy to 546 nm ($\Delta\bar{\nu} = 1070 \text{ cm}^{-1}$) in 2-Pt-6H. This is in striking contrast to the hypsochromic shift of 1600 cm^{-1} observed for the previously reported complex 8-Pt, where the platinum ion attaches to the *meso* position C8.⁶³ (TD)-DFT calculations explain this disparate behavior. Thus,

the HOMO of a bodipy dye has a nodal plane along the C8–B vector, whereas the LUMO has not. Hence, the electron-donating $\text{Pt}(\text{PR}_3)_2\text{I}$ fragment destabilizes the LUMO more than the HOMO, thereby increasing the HOMO–LUMO gap. In contrast, when bound to carbon atoms C2 or C3, the $\text{Pt}(\text{PR}_3)_2\text{I}$ moiety contributes more to the HOMO than to the LUMO, which decreases the HOMO–LUMO gap by 500 or 1100 cm^{-1} with respect to the free halogenated dye (Figures 3 and 4).

Similar to 8-Pt, the $\pi \rightarrow \pi^*$ band of 3-Pt is sharp, whereas it is broadened significantly in all of the 2-platinated bodipy complexes. Such broadening suggests a stronger perturbation of the bodipy π -system by the attached $\text{Pt}(\text{PET}_3)_2\text{I}$ fragment and additional underlying transitions resulting in richer absorption

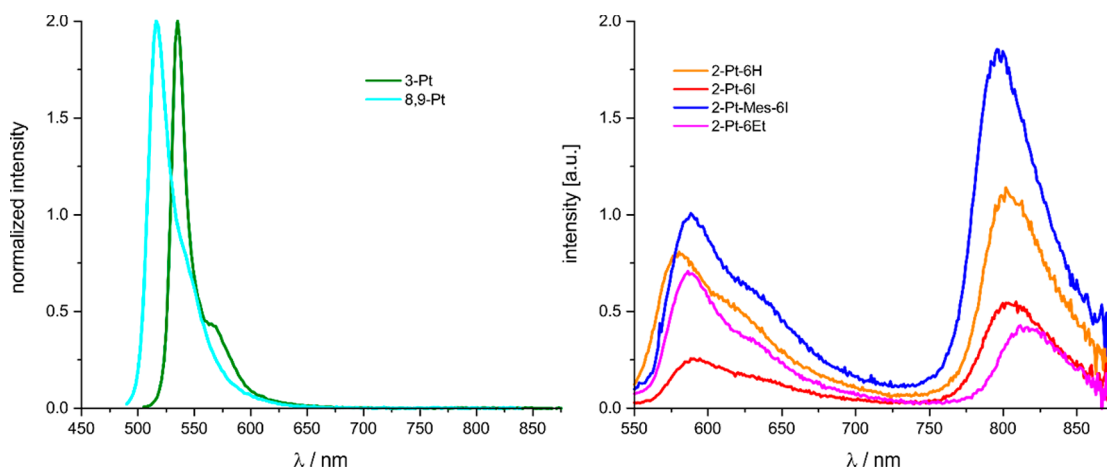


Figure 5. Left: Luminescence spectra of **3-Pt** (green) and **8,9-Pt** (cyan) in ca. 10^{-6} M toluene solution; right: luminescence spectra of **2-Pt-6H** (orange), **2-Pt-6I** (red), **2-Pt-Mes-6I** (blue), and **2-Pt-6Et** (magenta).

features. This is also borne out by our TD-DFT calculations on model complexes **3-Pt** and **2-Pt-Mes-6I**. Calculated and experimental spectra are compared in Figures S38 and S39, while Figures 3 and 4 display the crucial MOs and the computed transitions. Electron density difference maps (EDDMs) of the calculated transitions are also included as Figures S43 and S44; fragment contributions to the corresponding MOs according to Mulliken decomposition analysis are provided as Tables S3 and S4. Our calculations provide only a qualitative level of agreement with the experimental data (see Table 3) because the energies of the electronic transitions are overestimated by DFT methods. This is a known problem for bodipys and related cyanine dyes.^{33,34} Nevertheless, TD-DFT calculations agree with our experimental observations in predicting additional, rather intense HOMO-1/HOMO-3 \rightarrow LUMO transitions with PtI \rightarrow bodipy CT character for **2-Pt-Mes-6I** at rather close energies to the dominant $\pi \rightarrow \pi^*$ transition (see Table 3 and Figure 3). The latter have no equivalent in **3-Pt** (Figure 4) or **8-Pt**.⁵⁹ The predicted ML \rightarrow L'CT admixture to the high-energy part of this band still fails to cause any notable solvatochromism (see Figure S37a-d). A similar broadening of the HOMO \rightarrow LUMO absorption band of a Pt(bipy)(2-ethynylbodipy)₂ complex was recently observed by Zhong et al. and likewise attributed to MLCT and intraligand charge-transfer (ILCT) admixtures to the main $\pi \rightarrow \pi^*$ excitation.⁴¹ The results of our TD-DFT calculations for **3-Pt** provide an excellent match with the experimental spectrum in predicting a single, intense bodipy-based $\pi \rightarrow \pi^*$ band and additional ML \rightarrow L'CT and ILCT bands of only minor intensity in the UV (see Figures 4 and S39).

Luminescence Spectroscopy. As just discussed, changing the site of platinum attachment to the bodipy chromophore from *meso*/C8 to C2 or C3 gauges platinum contribution to the relevant frontier MOs and, in case of the 2-complexes, also mixes some PtI \rightarrow bodipy CT character into the main $\pi \rightarrow \pi^*$ absorption. One therefore expects that the positioning of the Pt(PeEt₃)₂I entity influences the ISC rates and emission energies as well as the relative intensities of the fluorescence and phosphorescence emissions. This is indeed the case.

Table 4 and Figure 5 summarize the luminescence properties of the new complexes as measured in gastight cuvettes under rigorous exclusion of air, along with those of the previously reported **8-Pt** as a point of comparison. The latter complex is

very weakly fluorescent but phosphoresces at 641 nm with a quantum yield of up to 41%.⁵⁹ Complexes **3-Pt** and **8,9-Pt** are strongly fluorescent in solution at r.t. (Φ_{Fl} ca. 50%) with an emission peak at 535 or 516 nm, respectively, but do not phosphoresce, even in a 2-MeTHF glass matrix at 77 K (Figures S45 and S46). Like in the absorption spectrum, platinum binding to the C=C double bond does not cause any appreciable shift of the emission wavelength with respect to 3-chloro-5,7-dimethyl-bodipy but decreases the quantum yield from 76 to 53%.⁶⁴

In contrast, the C2-platinated complexes exhibit dual luminescence with a fluorescence peak at 580–590 nm and phosphorescence in the near-infrared (NIR), at 797–815 nm. NIR phosphorescence of a bodipy dye at r.t. in fluid solution is a rather rare asset.^{26,30,41,65–67} Comparison of the excitation spectra recorded for the fluorescence and the phosphorescence emissions with the absorption spectra in Figure S47 proves that both emissions emanate from the same complex and that none of them is due to an impurity. As an unfortunate consequence of the small energy gap between the $^3\pi\pi^*$ and the S_0 states of the **2-Pt-bodipy** complexes and the concomitantly higher probability of radiationless decay to the ground state as expressed by the energy gap law,^{68,69} phosphorescence quantum yields are significantly smaller than those for **8-Pt**.

$$k_{\text{ISC}} = (1 - \Phi_{\text{Fl}}) / \tau_{\text{Fl}} - k_{\text{IC}} \quad (1)$$

$$k_{\text{ISC}} \leq (1 - \Phi) / \tau \quad (2)$$

ISC rate constants k_{ISC} were estimated from eq 2.⁷⁰ By assuming $k_{\text{IC}} \approx 0$ in eq 1 for all complexes, an upper limit for k_{ISC} is obtained.⁷⁰ Overall, the rate of ISC from the S_1 to the T_1 state follows the trend **8-Pt** > **2-Pt-6H,Et,I** > **3-Pt** (Table 4).

Comparison of the luminescence properties of the complexes **2-Pt-6H**, **2-Pt-6Et**, **2-Pt-6I**, and **2-Pt-Mes-6I** reveals that the substituent in 6-position at the second pyrrole ring, and, in particular, the presence of the iodine heavy atom or blocking the rotation of the *meso* aryl substituent, have only minor effects on the ISC rates, emission lifetimes, and, consequently, the relative intensities of the fluorescence and phosphorescence emissions. It was observed on other occasions that replacing the *meso* phenyl by a mesityl substituent serves to close channels for radiationless decay by rotation of the aryl substituent around the C8-aryl bond.^{71,72} In the case of complexes **2-Pt-6I** and **2-Pt-Mes-6I**, this modification also increases the QY of the NIR

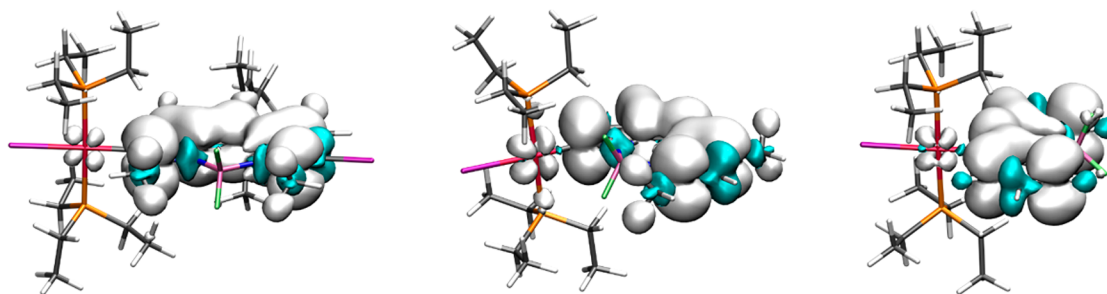
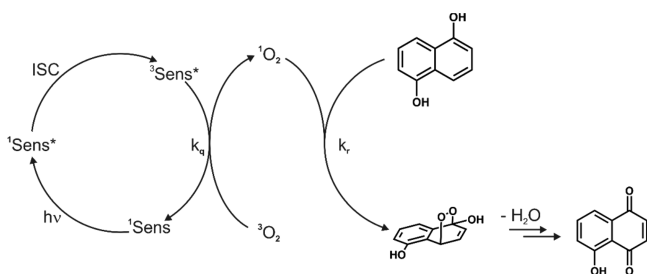


Figure 6. Spin density surfaces of the T_1 state of 2-Pt-Mes-6I (left), 3-Pt (middle), and 8-Pt (right).⁷³

phosphorescence emission, but it still remains very modest at 0.14%. Phosphorescence lifetimes of the 2-Pt-bodipy complexes range from 67 and 243 μ s at r.t. and increase significantly upon cooling to 77 K in a rigid 2-MeTHF matrix (Table 4). DFT calculations indicate that the fluorescence and phosphorescence emissions emanate from the $^1\pi\pi^*$ and $^3\pi\pi^*$ excited states of the bodipy ligand. Figure 6 shows that the spin density of the triplet state T_1 of complexes 8-Pt, 2-Pt-Mes-6I, and 3-Pt concentrates on the bodipy ligand with only minor contributions from the Pt(PET₃)₂I fragment (see also Table S5 for fragment contributions according to Mulliken).

An important asset of bodipy dyes is their potency to form 1O_2 from 3O_2 via TTA. This makes bodipys highly interesting sensitizers for applications in photocatalysis^{31,74–77} and photodynamic therapy (PDT).^{10,25,26,78,79} 8-Pt and its closely related *trans*-Pt(bodipy)Cl(PET₃)₂ analogue have shown up to almost unitarian quantum yields for photochemical 1O_2 generation with no signs of decomposition over 3 h. The model photooxidation of 1,5-dihydroxynaphthalene (DHN) to Juglone pursuant to Scheme 2 was monitored by recording

Scheme 2. Photooxidation of DHN to Juglone with 1O_2 in the Presence of a Photosensitizer



UV/vis spectra at regular intervals during photoirradiation and calculating the pseudo first-order kinetics for DHN consumption (for details see the Experimental Section and Figures S48–S52). Slight deviations of the slopes when plotting $\ln(C_t/C_0)$ as a function of time t after 60 min mark the onset of photodecomposition.

Table 5 summarizes the results of these experiments. Complexes of the 2-Pt series reach only modest quantum yields of 53 and 34%. Still, DHN oxidation to Juglone occurs with higher turnover frequencies (TOFs) than for 8-Pt as a result of a better overlap of their absorption envelopes with the radiation of the light source as expressed by the higher value of I (Table 5). Although 3-Pt is nonphosphorescent, its excited triplet state is still populated to an appreciable extent. This follows from the reduction of the fluorescence lifetime τ_{FI} compared to 3-chloro-5,7-dimethyl-bodipy (5.46 ± 0.01 ns)⁶⁴ and from the 1O_2 quantum yield of 19% using 3-Pt as the sensitizer. We suspect that the substantially lower quantum yields of the present complexes for 1O_2 generation when compared to 8-Pt are also rooted in the comparatively low energies of their T_1 states, which renders energy transfer to 3O_2 less exergonic while making decay by other pathways more efficient. In summary, we note that the QYs for 1O_2 generation mirror the trend for the ISC rates and decrease from 8-Pt to the 2-platinated complexes and to 3-Pt, paralleling the trends obtained from luminescence spectroscopy (vide supra).

In order to probe whether DHN oxidation occurs preferably via the direct reductive quenching of the excited state of the complexes with DHN as the electron donor or by energy transfer to 3O_2 and the subsequent reaction of DHN with photogenerated 1O_2 we exemplarily monitored the phosphorescence quenching of 2-Pt-Mes-6I with oxygen or DHN as the quencher. Stern–Volmer plots and stack plots showing the emission intensities and decays without or with the respective quencher at various concentration levels are provided as Figures

Table 5. Pseudo First-Order Kinetics, 1O_2 Generation Quantum Yields, and Turnover Frequencies for the DHN Photooxidation Using the Complexes 8-Pt,⁵⁹ 2-Pt-6H, 2-Pt-6I, 2-Pt-Mes-6I, 2-Pt-6Et, 3-Pt, and Methylene Blue (MB) as Sensitizers

	λ_{ex} (nm)	k_{obs} (min ⁻¹) ^a	ν_i ($\times 10^{-6}$ M min ⁻¹) ^b	I^c	Φ_{Δ}^d	yield (%) ^e	TOF (s ⁻¹) ^f
8-Pt	460 \pm 5	0.00145	0.1757	0.810	0.95	25	0.0014
2-Pt-6H	550 \pm 5	0.00377	0.4649	3.988	0.51	35	0.0037
2-Pt-6I	550 \pm 5	0.00413	0.5093	4.221	0.53	24	0.0025
2-Pt-Mes-6I	550 \pm 5	0.00449	0.5130	4.665	0.48	26	0.0029
2-Pt-6Et	550 \pm 5	0.00344	0.4242	5.462	0.34	23	0.0024
3-Pt	530 \pm 5	0.00337	0.4155	9.557	0.19	26	0.0027
MB	655 \pm 5	0.00102	0.1296	1	0.57	5	0.0003

^aPseudo-first-order rate constant for DHN consumption. ^bInitial rate of DHN consumption. ^cRelative number of photons absorbed by the sensitizer ($I = 1$ for the standard sensitizer MB). ^dCorrected 1O_2 generation quantum yields using the value of MB ($\Phi_{\Delta} = 0.57$)^{81–83} as a reference. ^eYield of Juglone after a reaction time of 60 min. ^fTurnover frequency.

S53–S58. With a Stern–Volmer quenching constant K_{SV} of $2150 \pm 200 \text{ bar}^{-1}$ or $670 \pm 61 \mu\text{M}^{-1}$, the phosphorescence emission of **2-Pt-Mes-6I** was found to be almost as sensitive to oxygen as that of **8-Pt** ($K_{SV} = 2580 \pm 71 \text{ bar}^{-1}$).⁵⁹ The quenching constant for DHN as the quencher is smaller by a factor of 22 ($K_{SV} = 31 \pm 2 \mu\text{M}^{-1}$), which identifies energy transfer as the dominant pathway. In agreement with that, quenching by electron transfer is calculated to be endergonic by 1.01 eV (97.5 kJ/mol) based on the Rehm–Weller equation (see also Figure S59 for the peak potential of electrochemical DHN oxidation).⁸⁰ Similar values were derived for the other complexes so that this statement should apply for these as well.

Electrochemistry and UV/Vis/NIR and EPR Spectroelectrochemistry. Bodipys are generally electroactive and can be oxidized and reduced by one electron each.^{41,53,54,56} Their associated radical cations or anions are sometimes sufficiently persistent to allow for their spectroscopic characterization by UV/vis/NIR^{84–90} or EPR spectroscopy.⁹¹ Such investigations are particularly relevant for the spectroscopic identification of bodipy radical species in the photoexcited, charge-separated states. Examples are dyads or triads, where a bodipy is linked to a peripheral 2,4,5-trimethoxybenzene,⁸⁵ phenylanthracene,⁸⁶ triarylamine⁸⁷ or *N*-(2-ethylhexyl)dithieno[3,2-*b*:2',3'-*d*]pyrrole (DTP)⁹² electron donor or a fullerene⁸⁹ or carborane acceptor.⁹⁰ The latter are of great interest with respect to light-to-energy conversion schemes or mimicking natural enzymes.^{85,87,90,92,93}

The results of our voltammetric studies on the σ -platinum bodipy complexes are summarized in Table 6. In their cyclic

Table 6. Electrochemical Data for all Complexes and Representative Halogenated Bodipys^a

complex	$E_{1/2}$	$E_{1/2}$
	0/+	0/-
8-Br-bodipy		-1530
8-Mes-2,6-I₂-bodipy	890	-1520
3-Cl-bodipy	950	-1420
2-Pt-6H	450	-1920
2-Pt-6I	540	-1810
2-Pt-Mes-6I	540	-1860
2-Pt-6Et	370	-1960
3-Pt	410	-1930
8-Pt		-1770

^aAll potentials are given in mV relative to the $\text{Cp}_2\text{Fe}^{0/+}$ couple ($E_{1/2} = 0.000 \text{ V}$) and were measured in CH_2Cl_2 at 293 K with NBu_4PF_6 as the supporting electrolyte.

voltammograms, all complexes except for **8-Pt** show a fully or nearly reversible one-electron oxidation and a reversible to partially reversible reduction within the electrochemical window of the $\text{CH}_2\text{Cl}_2/\text{NBu}_4\text{PF}_6$ supporting electrolyte (see Figures 7 and 8). Figure S60 illustrates the voltammetric traces of the 8-mesityl-2,6-diiodobodipy, 3-chloro-5,7-dimethylbodipy, and 8-bromo-bodipy precursors under the same conditions as points of comparison. For the latter two compounds, higher sweep rates were required in order to outrun chemical follow processes following oxidation or reduction. Similar to related bis(phosphane) platinum alkynyl complexes containing 2- or 8-ethynylated bodipy ligands,^{33,35} attachment of the electron-rich platinum entity causes sizable cathodic shifts of both redox waves. The cathodic shift of 450–540 mV for the 0/+ redox couple on platinum attachment to

the bodipy carbon atom C2 or C3 slightly surpasses that of 340–510 mV for the 0/- process (Table 6). This is consistent with the higher contribution of the $\text{Pt}(\text{PEt}_3)_2\text{I}$ fragment to the HOMO (c. f. Figures 3 and 4 and Tables S3 and S4).

The oxidation (0/+) or reduction (0/-) half-wave potentials also trace the degree of the electronic interaction of the $\text{Pt}(\text{PR}_3)_2\text{I}$ -fragment with the bodipy chromophore. Attachment to the *meso*-position C8 causes a smaller potential difference $\Delta E_{1/2}$ of 240 mV with respect to the parent dye than platinum attachment to carbon atom C2 ($\Delta E_{1/2} = 340 \text{ mV}$) or C3 ($\Delta E_{1/2} = 510 \text{ mV}$; note, however, that the presence of a chloro substituent in **3-Cl-bodipy** instead of the iodo substituent in the other dyes likely contributes to the increased potential shift of **3-Pt**). Exchanging the substituent in 6-position of the 2-platinated dyes has a similar effect on both half-wave potentials and causes a cathodic shift with increasing electron donating capability in the ordering $\text{Et} > \text{H} > \text{I}$.

All our previous data indicate that the HOMO and LUMO of the platinum σ -bodipy complexes are dominated by the bodipy ligand. Monitoring the changes in the UV/vis/NIR spectra on one-electron reduction or oxidation provides a direct means to experimentally probe for the identity of the corresponding redox site. Some accounts of spectroelectrochemical investigations on bodipy dyes have already appeared in the literature. The results of these studies can serve as reference points for our present results.^{84,85,87,89,91,92,94,95} Like for the other studies, the radical cations or anions were generated inside a transparent UV/vis/NIR cell⁹⁶ or inside an EPR tube under the in situ conditions of spectroelectrochemistry. The results of these studies are displayed in Figures 9 and S61–S63, while Table 7 summarizes the relevant data and the TD-DFT calculated band energies and assignments. Plots of the pertinent MOs and transitions along with the corresponding electron density difference maps (EDDMs) of the oxidized and reduced forms of representative complexes as well as fragment contributions according to Mulliken analysis can be retrieved from Figures S64–S71 and Tables S7–S10.

As it was previously observed for other bodipy dyes, the prominent $\pi \rightarrow \pi^*$ band partially bleaches on reduction while a new, weaker absorption band grows in. The latter is by ca. 40–50 nm to the red from the former HOMO \rightarrow LUMO band (see Figures 9a–c, S61a, and S62a). According to our TD-DFT results, the new low-energy band of the radical anions is assigned as a bodipy \rightarrow $\text{Pt}(\text{PEt}_3)_2$ CT transition (see Table 7, Figures S64, S65, and S68–S71). As shown in Figure S62a, the reduction of 8-mesityl-2,6-diiodo-bodipy produces nearly identical spectroscopic changes. All reduction processes are highly reversible as shown by the multiple isosbestic points and the nearly complete recovery of the original spectra after a full reduction/reoxidation cycle (c.f. Figures S62b and S63).

On the time scale of spectroelectrochemical experiments, only **2-Pt-Mes-6I** (Figures 9d and S63e) and **2-Pt-6Et** (Figure S61b and S63f) can be reversibly oxidized. Concomitant with the bleaching of the characteristic $\pi \rightarrow \pi^*$ transition, a weak, broad NIR band enveloping the entire regime between 750 and 1750 nm is observed. This again agrees with previous studies on other bodipys.^{87,88,94,95} TD-DFT calculations suggest that the NIR absorption of the **2-Pt-Mes-6I** radical cation originates from a mixed ILCT (Mes \rightarrow bodipy) and $\text{PtI} \rightarrow$ bodipy ML \rightarrow L/CT transition at 1162 nm and at 805 nm with CT from the iodo and mesityl substituents to the bodipy π system (see Figures S66 and S67 and Table 7).

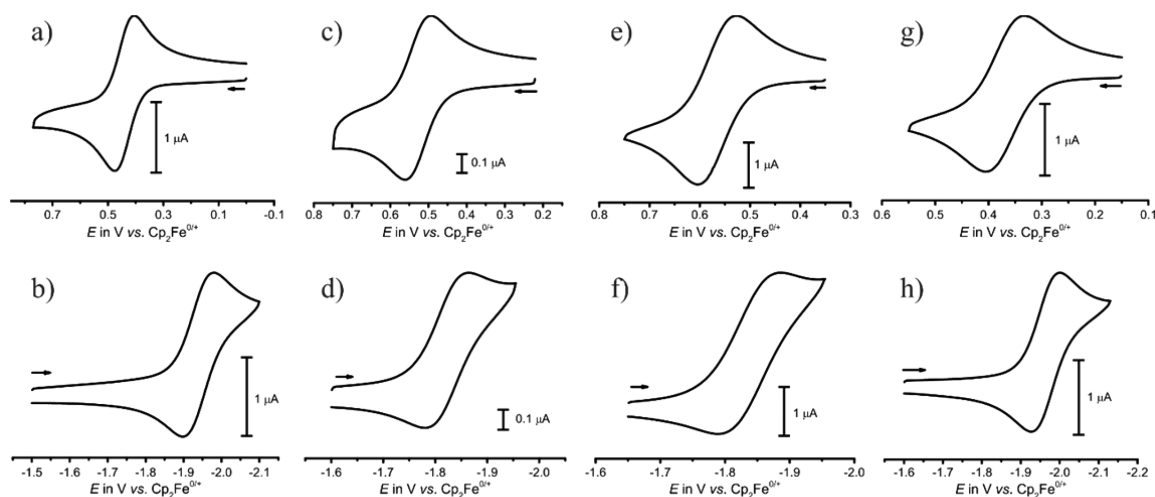


Figure 7. Cyclic voltammograms ($\nu = 100$ mV/s) recorded for anodic (top) and cathodic (bottom) sweeps of (a, b) **2-Pt-6H**, (c, d) **2-Pt-6I**, (e, f) **2-Pt-Mes-6I**, and (g, h) **2-Pt-6Et** in CH_2Cl_2 at $T = 293$ K with NBu_4PF_6 (0.1 M) as the supporting electrolyte.

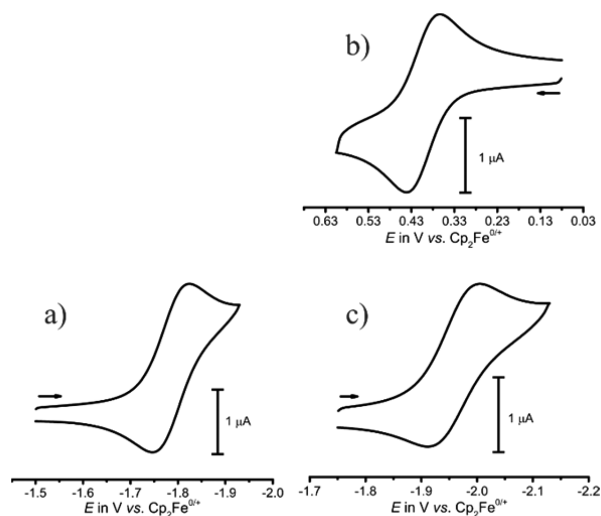


Figure 8. Cyclic voltammograms recorded for anodic (top) and cathodic (bottom) sweeps of (a) **8-Pt** ($\nu = 100$ mV/s) and (b, c) **3-Pt** ($\nu = 200$ mV/s) in CH_2Cl_2 solution at $T = 293$ K with NBu_4PF_6 (0.1 M) as the supporting electrolyte.

Owing to the presence of multiple nuclei with a nuclear spin $I \neq 0$, and the fundamental differences between ligand- and metal-centered spin, EPR spectroscopy provides another potent tool to probe for the identity of the respective redox site. In particular, the hyperfine splittings (hfs) to the abundant (33.8%) ^{195}Pt $I = 1/2$ nucleus provides a means for probing the platinum contribution to the relevant SOMO. We note that EPR spectroscopic investigations on bodipy-derived radical cations or anions are extremely rare.⁹¹ The radical forms of all compounds were prepared by electrochemical oxidation or reduction inside an EPR tube using a three-electrode configuration. EPR spectra of the one-electron reduced forms of the complexes **2-Pt-Mes-6I**, **3-Pt**, and **8-Pt** as well as those of oxidized **2-Pt-Mes-6I** and **3-Pt** are displayed in Figures 10–12. Comparison with the EPR spectra of the oxidized and reduced forms of the 8-mesityl-2,6-diiodo-bodipy precursor (see Figure S72) aids in the identification of the ^{195}Pt and ^{31}P hfs.

The radical cation of 8-mesityl-2,6-diiodo-bodipy gives a partially resolved EPR spectrum at a g -value of 2.0042. The

EPR spectra of the radical cations of the Pt complexes are broader but exhibit clearly resolved hfs to the platinum nucleus of the ^{195}Pt -containing isotopomer. At 100.9 G, the value of the 2-platinated complex **2-Pt-Mes-6I** is larger than that of 81.7 G for **3-Pt**. As a result of the minor metal contribution to the SOMO (for calculated spin densities, see Figures 13 and 14, and for fragment analysis, see Tables S7–S10), the g -values are only moderately increased with respect to the Landé factor g_e of 2.002319 of the free electron and that of the 8-mesityl-2,6-diiodo-bodipy radical cation.

Quite remarkably, the EPR spectrum of the **8-Pt** radical anion is entirely dominated by hyperfine interactions with ^{31}P and the ^{195}Pt nuclei of the $\text{Pt}(\text{PEt}_3)_2$ fragment (see Figure 10, Table 8). Calculated spin densities are displayed in Figure S73, while a fragment analysis is provided in Table S11. The EPR spectra of the radical anions of free dyes and associated platinum complexes **2-Pt-Mes-6I** and **3-Pt** offer an even richer structuring due to resolved hfs to the ^{14}N , $^{10/11}\text{B}$, and ^{19}F nuclei (see Figures 13 and 14 for calculated spin density distributions). Comparison of the spectra of the 8-mesityl-2,6-diiodo-bodipy radical anion (see Figure S72 and Table S11 for calculated spin density distributions) with those of reduced **2-Pt-Mes-6I** and **3-Pt** evidence the presence of hfs interactions with the ^{195}Pt nucleus in the latter. Spectra simulated with the hfs constants compiled in Table 8 are also displayed in Figures 10–12 and S72. Despite the overall good agreement between experimental and simulated spectra, the multitude of possible hfs interactions render our simulations and assignments of hfs constants only tentative. Again, the g -values of the reduced complexes (1.9917–1.9993) are close to that of 1.9935 for the 8-mesityl-2,6-diiodo-bodipy radical anion. This again confirms the organic parentage of these paramagnetic species.

In summary, the close resemblance of the UV/vis/NIR and EPR spectra of the oxidized and reduced forms of 8-mesityl-2,6-diiodo-bodipy and related bodipy dyes to those of the electrogenerated radical cations and anions of the σ -bodipy platinum complexes fully agrees with our conclusions derived from their optical and photophysical properties and reconfirms that their HOMOs and LUMOs are largely based on the bodipy ligands.

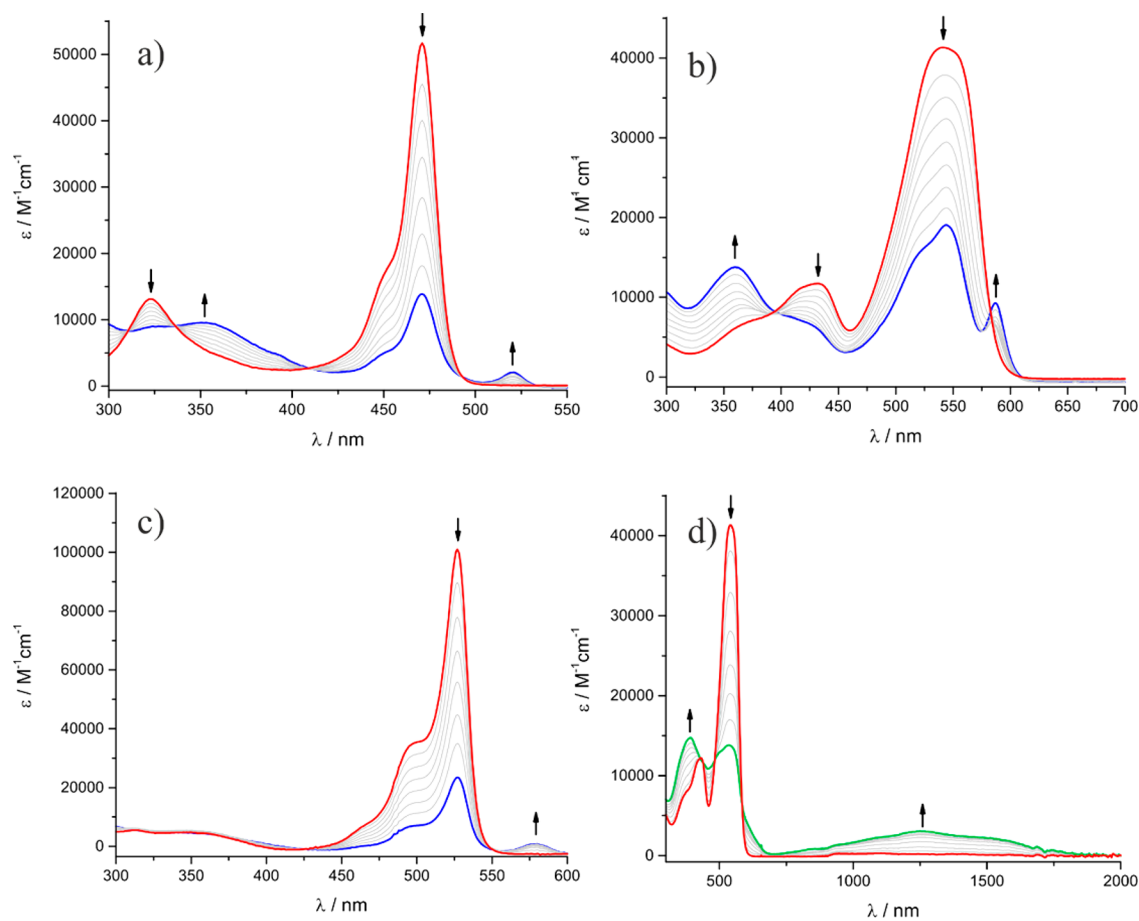


Figure 9. Changes of the UV/vis/NIR spectra ($1,2\text{-C}_2\text{H}_4\text{Cl}_2$, NBu_4PF_6 , $T = 293 \text{ K}$) on (a) reduction of **8-Pt**, (b) reduction of **2-Pt-Mes-6I**, (c) reduction of **3-Pt**, and (d) oxidation of **2-Pt-Mes-6I**.

SUMMARY AND CONCLUSIONS

Five new platinum bodipy complexes, where a *trans*-Pt(PEt₃)₂I moiety attaches to the pyrrolic carbon atom C2 or C3 of a bodipy dye via a direct Pt–bodipy σ -bond have been prepared. They complement previous series of complexes where a *trans*-Pt(PR₃)₂X (R = Ph, X = Br; R = Et, X = Cl, Br, I, NCS, NO₂, and CH₃) entity binds to the *meso* bodipy position C8.^{59,63} The higher activation barrier for oxidative addition of the Pt(PEt₃)₂ fragment to a C_{aryl}–Cl bond as compared to a C_{aryl}–I bond has also allowed us to isolate complex **8,9-Pt** as a direct precursor to complexes *cis/trans* **3-Cl-Pt**, Pt–Cl analog of the iodo complex **3-Pt**. Thermal conversion of **8,9-Pt** to **3-Cl-Pt** and the gradual (yet incomplete) *cis* \rightarrow *trans* isomerization of **3-Cl-Pt** were followed by ³¹P NMR spectroscopy. The spectroscopic, structural, photophysical, and electrochemical properties of all complexes were studied and compared to those of the *meso*-substituted complex **8-Pt** and the corresponding bodipy precursors. Contrary to **8-Pt**, platinum attachment to either position C2 or C3 puts the Pt(PEt₃)₂I entity within the conjugated π -system and thus induces a sizable red shift of the characteristic bodipy absorption band along with a broadening for the 2-isomers. Its dominant bodipy $\pi \rightarrow \pi^*$ character is retained as inferred from the DFT-calculated frontier MOs and the TD-DFT based band assignments.

All complexes can be oxidized or reduced by one electron each as probed by cyclic voltammetry. Introduction of the electron-donating Pt(PEt₃)₂I entity causes strong cathodic shifts of 340–510 mV for both oxidation and reduction. UV/

vis/NIR and EPR spectroelectrochemistry allowed for spectroscopic characterization of the persistent radical anions and of some sufficiently stable radical cations of the complexes and provides direct experimental evidence for ligand-centered frontier MOs. Thus, their UV/vis/NIR spectroscopic patterns are very similar to those of the one-electron oxidized or reduced forms of their bodipy precursors. Moreover, richly structured EPR spectra with resolved hfs to heteronuclei (¹⁹⁵Pt, ³¹P, ¹⁴N, and ¹⁹F) with *g* values close to *g*_e have been recorded and attest to a dominantly organic spin, again in full agreement with DFT calculated spin density distributions.

Like **8-Pt**, all complexes where the Pt ion is bonded to carbon atom C2 dually emit through fluorescence and phosphorescence with phosphorescence emission well in the NIR, at 797–815 nm. However, quantum yields are severely reduced from 41% in **8-Pt** to meager values of 0.14% or less. Nevertheless, all complexes are active sensitizers for photochemical ¹O₂ generation and outperform methylene blue as a catalyst for the photooxidation of 1,5-dihydroxynaphthalene to Juglone. Our present results show that attachment to either the 2- or 3-positions is no viable route to Pt–bodipy dyes with intense NIR phosphorescence emission. It remains to be investigated whether such compounds are accessible from appropriately substituted 8-bromo (*meso*) bodipys with extended π -conjugation at the pyrrole rings. Work along these lines is presently being pursued in our laboratories.

Table 7. UV/Vis/NIR Data^a of the Oxidized and/or Reduced Forms of Complexes 8-Pt, 2-Pt-Mes-6I, 2-Pt-6Et, and 3-Pt and TD-DFT Calculated Data (PBE1PBE/6-31G(d), PCM (CH₂Cl₂))

compound	absorption data			TD-DFT data			assignment
	ox. state	$\lambda_{\text{max}}/\text{nm}$ ($\epsilon/\text{L mol}^{-1} \text{cm}^{-1}$)	ox. state	λ (nm)	f	major contributions	
8-Pt	-	520 (2100), 471 (13900), 352 (9500)	-	677	0.002	HOMO(α) \rightarrow LUMO(α) (91%) HOMO(β) \rightarrow LUMO(β) (81%)	LMCT ^c $\pi \rightarrow \pi^*$
8-Mes-2,6-I ₂ -bodipy	-	562 (15800), 534 (22500), 356 (17700), 306 (16200)	n.c. ^b	433	0.069		
2-Pt-Mes-6I	+	1260 (3000), 538 (13800), 391 (14700)	+	1162	0.09	H-2(β) \rightarrow LUMO(β) (33%), HOMO(β) \rightarrow LUMO(β) (43%)	ML \rightarrow L'CT ^d , ILCT ^e
	-	587 (9300), 544 (19000), 360 (13800)	-	805	0.05	H-6(β) \rightarrow LUMO(β) (27%), H-5(β) \rightarrow LUMO(β) (59%) (31%), HOMO(β) \rightarrow LUMO(β) (55%), HOMO(α) \rightarrow L+2(α)	ILCT ^e $\pi \rightarrow \pi^*$ with metal contribution
2-Pt-6Et	+	1211 (2500), 555 (12100), 381 (18700)	n.c. ^b	507	0.14		
	-	603 (6900), 556 (25100), 361 (12400)		501	0.08	HOMO(α) \rightarrow L+2(α) (27%), HOMO(α) \rightarrow L+3(α) (24%), HOMO(α) \rightarrow L+4(α) (15%)	ILCT ^e with metal contribution
3-Pt	-	580 (900), 527 (23500), 350 (4700)	-	584	0.002	HOMO(α) \rightarrow LUMO(α) (91%) HOMO(β) \rightarrow LUMO(β) (90%)	LMCT ^c $\pi \rightarrow \pi^*$

^aAll band positions are given in nm, and extinction coefficients are given in L mol⁻¹ cm⁻¹. Measured in 1,2-C₂H₄Cl₂. ^bn.c. = Not calculated. ^cLMCT = ligand to metal charge transfer. ^dML \rightarrow L'CT = metal/ligand to ligand' charge transfer. ^eILCT = intra ligand charge transfer.

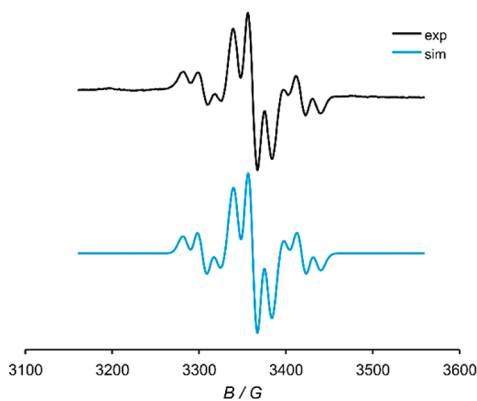


Figure 10. Experimental (top curve) and simulated (bottom curve) EPR spectra of the radical anion of **8-Pt** in $\text{CH}_2\text{Cl}_2/\text{NBu}_4^+\text{PF}_6^-$ at 248 K.

EXPERIMENTAL SECTION

Materials and Methods. The oxidative addition reactions were performed under a N_2 atmosphere using standard Schlenk techniques or inside a glovebox. The *cis/trans* isomerization reactions and workup were conducted in air. C_6D_6 , CD_2Cl_2 , CDCl_3 and $\text{THF-}d_8$ were supplied from Eurisotop. Compounds **6-H-bodipy**,⁹⁷ **6-I-bodipy**,⁹⁷ **2,6-I₂-bodipy**,⁹⁷ **2,6-I₂-8-Mes-bodipy**,^{53,98} **6-Et-bodipy**,⁹⁹ **3-Cl-bodipy**,^{100,101} and $\text{Pt}(\text{Et})_2(\text{PEt}_3)_2$ were synthesized according to literature protocols. NMR experiments were carried out on a Varian Unity Inova 400, a Bruker Avance III DRX 400, or a Bruker Avance DRX 600 spectrometer. ^1H and ^{13}C spectra were referenced to the solvent signal, while ^{31}P and ^{195}Pt spectra were referenced to external standards (85% H_3PO_4 or saturated $\text{K}_2[\text{PtCl}_6]$ in D_2O , respectively). NMR data are given as follows: chemical shift (δ in ppm), multiplicity (br, broad; d, doublet; dd, doublet of doublets; m, multiplet; s, singlet; t, triplet; vt, virtual triplet), integration, and coupling constant (Hz). Unequivocal signal assignments were achieved by 2D NMR experiments. The numbering of the nuclei follows that of the chemical structures in Figure 1. Combustion analysis was conducted with an Elementar vario MICRO cube CHN-analyzer from Heraeus.

X-ray diffraction analysis of single crystals was performed at 100 K on a STOE IPDS-II diffractometer equipped with a graphite-monochromated radiation source ($\lambda = 0.71073 \text{ \AA}$) and an image plate detection system. A crystal mounted on a fine glass fiber with silicon grease was employed. If not indicated otherwise, then the selection, integration, and averaging procedure of the measured reflection intensities, the determination of the unit cell dimensions and a least-squares fit of the 2θ values as well as data reduction, LP-correction and space group determination were performed using the

X-Area software package delivered with the diffractometer. A semiempirical absorption correction was performed.¹⁰² All structures were solved by the heavy-atom methods (SHELXS-97,¹⁰³ SHELXS-2013,¹⁰⁴ SHELXS-2014,¹⁰⁵ or OLEX2¹⁰⁶). Structure solutions were completed with difference Fourier syntheses and full-matrix least-squares refinements using SHELXL-97,¹⁰³ SHELXS-2013,¹⁰⁴ SHELXS-2014,¹⁰⁵ or OLEX2¹⁰⁶ minimizing $\omega(F_o^2 - F_c^2)^2$. The weighted R factor (wR^2) and the goodness of the fit GOF are based on F^2 . All non-hydrogen atoms were refined with anisotropic displacement parameters, while hydrogen atoms were treated in a riding model. Molecular structures in this work are plotted with PLATON¹⁰⁷ or Mercury.¹⁰⁸ CIF files of the complexes have been deposited at the Cambridge Structure Data Base as CCDC 1583642 (**2-Pt-6H**), CCDC 1583615 (**2-Pt-6I**), CCDC 1583616 (**2-Pt-Mes-6I**), CCDC 1583637 (**2-Pt-6Et**), CCDC 1583640 (**8,9-Pt**), and CCDC 1583638 (**3-Pt**) and can be obtained free of charge via www.ccdc.cam.ac.uk/conts/retrieving.html or from the Cambridge Crystallographic Data Center, 12 Union Road, Cambridge CB2 1EZ, U.K.; fax (+44)1223-336-033, or at deposit@ccdc.cam.ac.uk. Luminescence spectra and lifetimes as well as quantum yields were measured on thoroughly deaerated solutions (three freeze-pump-thaw cycles in a quartz cuvette equipped with an angle valve from Normag) of the complexes in CH_2Cl_2 , 2-MeTHF, or toluene solutions on a PicoQuant FluorTime 300 spectrometer. Unless stated otherwise absolute quantum yields were determined with an integrating sphere. UV/vis/NIR spectra were recorded on a TIDAS fiber optic diode array spectrometer (combined MCS UV/NIR and PGS NIR instrumentation) from J&M in HELMA quartz cuvettes with 0.1 cm optical path lengths. Electron paramagnetic resonance (EPR) experiments were performed on a MiniScope MS400 table-top X-band spectrometer from Magnettech. Simulation of the experimental EPR spectra was performed with the MATLAB EasySpin program.¹⁰⁹ All electrochemical experiments were executed in a home-built cylindrical vacuum-tight one-compartment cell. A spiral shaped Pt wire and an Ag wire as the counter and pseudoreference electrodes are sealed into glass capillaries and fixed by quickfit screws via standard joints. A platinum electrode is introduced as the working electrode through the top port via a Teflon screw cap with a suitable fitting. It is polished first with 1 μm diamond paste and then 0.25 μm diamond paste before measurements. The cell may be attached to a conventional Schlenk line via a side arm equipped with a Teflon screw valve, allowing experiments to be performed under an argon atmosphere with approximately 5–7 mL of analyte solution. NBu_4PF_6 (0.1 mM) was used as the supporting electrolyte. Referencing was done with addition of an appropriate amount of decamethylferrocene (Cp^*_2Fe) as an internal standard to the analyte solution after all data of interest had been acquired. Representative sets of scans were repeated with the added standard. Electrochemical data were acquired with a computer-controlled BASi CV50 potentiostat. The optically transparent thin-layer electrochemical (OTTLE) cell was lab-built and followed the design of Hartl and co-workers.⁹⁶ It

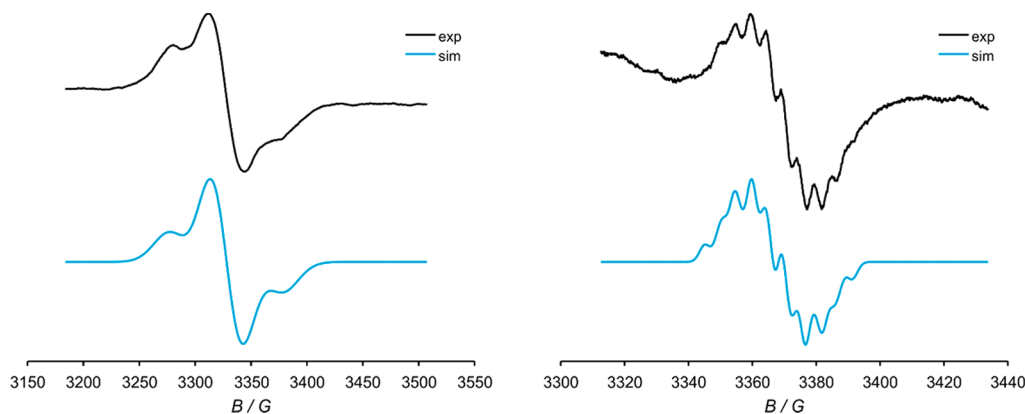


Figure 11. Experimental (top curve) and simulated (bottom curve) EPR spectra of the radical cation (left) and the radical anion (right) of **2-Pt-Mes-6I** in $\text{CH}_2\text{Cl}_2/\text{NBu}_4\text{PF}_6$ at 248 K.

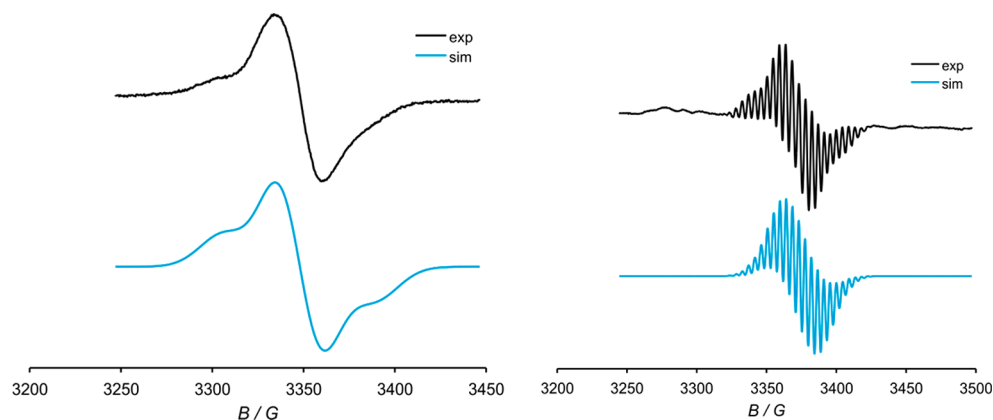


Figure 12. Experimental (top curve) and simulated (bottom curve) EPR spectra of the radical cation (left) and the radical anion (right) of complex 3-Pt in $\text{CH}_2\text{Cl}_2/\text{NBu}_4\text{PF}_6$ at 233 K.

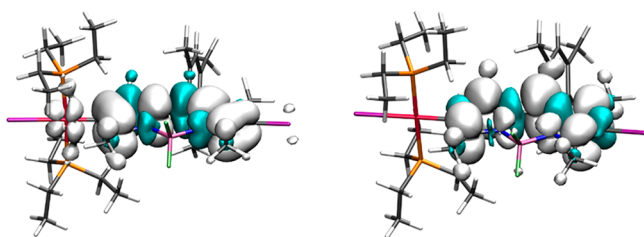


Figure 13. Calculated spin densities of the radical cation (left) and the radical anion (right) of 2-Pt-Mes-6I (PBE1PBE/6-31G(d) PCM (CH_2Cl_2)).

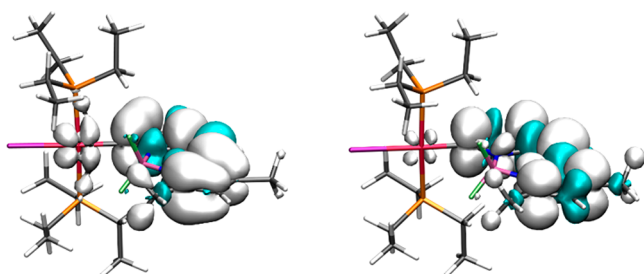


Figure 14. Calculated spin densities of the mono-cationic (left) and mono-anionic (right) form of 3-Pt (PBE1PBE/6-31G(d) PCM (CH_2Cl_2)).

comprised a Pt working and counter electrode and a thin silver wire as a pseudoreference electrode sandwiched in between two CaF_2 windows of a conventional liquid IR cell with the working electrode positioned in the center of the spectrometer beam.

Computational Details. The ground-state electronic structures were calculated by density functional theory (DFT) methods using the

Gaussian 09¹¹⁰ program package. Quantum-chemical studies were performed without any symmetry constraints. Open-shell systems were calculated by the unrestricted Kohn–Sham approach.¹¹¹ Geometry optimizations followed by vibrational analysis were performed either in a vacuum or in solvent media. The quasi-relativistic Wood–Boring small-core pseudopotentials (MWB),^{112,113} the corresponding optimized set of basis functions¹¹⁴ for platinum and the halogen atoms, and the 6-31G(d)-polarized double- ζ basis set¹¹⁵ for the remaining atoms were employed together with the Perdew–Burke–Ernzerhof exchange and correlation functional (PBE0).^{116,117} Solvent effects were accounted for by the polarizable conductor continuum model (PCM)^{118–121} with standard parameters for dichloromethane. Absorption spectra and orbital energies were calculated using time-dependent DFT (TD-DFT)¹²² with the same functional/basis set combinations as those mentioned above. For an easier comparison with the experiment, the obtained absorption and emission energies were converted into wavelengths and broadened by a Gaussian distribution (full width at half-maximum = 3000 cm^{-1}) using the program GaussSum.¹²³ Atomic coordinates of the calculated structures are provided as a separate file in the [Supporting Information](#).

¹O₂ Generation from Sensitizers. For the photoreactions involving ¹O₂ generation, a $\text{CH}_2\text{Cl}_2/\text{MeOH}$ (9/1) solution containing DHN ($1.2 \times 10^{-4}\text{ M}$) and a sensitizer (1.7 mol % vs DHN) was irradiated in a quartz cell of 1 cm path length using the xenon lamp of a PicoQuant FluorTime 300 spectrometer ($\lambda_{\text{exc}}(3\text{-Pt}) = 530 \pm 5\text{ nm}$, $I_f(530 \pm 5\text{ nm}) = 2.40\text{ mW}$; ($\lambda_{\text{exc}}(2\text{-Pt-6H, 2-Pt-6I, 2-Pt-Mes-6I, 2-Pt-6Et}) = 550 \pm 5\text{ nm}$, $I_f(550 \pm 5\text{ nm}) = 2.37\text{ mW}$; $\lambda_{\text{exc}}(\text{MB}) = 655 \pm 5\text{ nm}$, $I_f(655 \pm 5\text{ nm}) = 580\text{ }\mu\text{W}$). UV–vis absorption spectra were recorded at intervals of 5–20 min on a Varian Cary 50 spectrometer. The consumption of DHN was monitored by the decrease in absorption at 301 nm ($\epsilon = 7664\text{ M}^{-1}\text{ cm}^{-1}$),¹²⁴ while Juglone production was monitored by an increase of the absorption at 427 nm ($\epsilon = 3811\text{ M}^{-1}\text{ cm}^{-1}$).¹²⁴ The yield of Juglone was calculated from the

Table 8. EPR Data of 8-Pt, 8-Mes-2,6-I₂-bodipy, 2-Pt-Mes-6I, and 3-Pt^a

	<i>q</i>	<i>g</i> -value	$A(^{195}\text{Pt})^b$	$A(^{31}\text{P})^b$	$A(^{14}\text{N})^{b,c}$	$A(^{10/11}\text{B})^b$	$A(^{19}\text{F})^b$	$A(^{127}\text{I})^b$
8-Pt	–	1.9993	153.8 (1)	21.6 (2)				
8-Mes-2,6-I ₂ -bodipy	+	2.0042			9.6 (2)	11.1 (1)	9.6 (2)	
	–	1.9935			12.4 (2)		6.2 (2)	
2-Pt-Mes-6I ^c	+	2.0194	100.9 (1)					
	–	1.9955		12.0 (2)	5.8 (1), 3.4 (1)		8.2 (2)	
3-Pt ^c	+	2.0075	81.7 (1)					
	–	1.9917	37.5 (1)		7.2 (1), 5.3 (1)	5.8 (1)	11.1 (2)	5.8 (1)

^aIn CH_2Cl_2 solution; all hyperfine coupling constants are given in G. ^bThe number of interacting nuclei is given in parentheses. ^cUnsymmetrically substituted complexes give two different hyperfine couplings for the two ¹⁴N nuclei.

concentration of Juglone and the initial concentration of DHN. The singlet oxygen quantum yield (Φ_{Δ}) was determined using eq 3.^{124,125}

$$\Phi_{\Delta} = \Phi_{\Delta, \text{std}} (v_{I, \text{std}}/v_{I, \text{std}}) \quad (3)$$

where $\Phi_{\Delta, \text{std}}$ is the singlet oxygen quantum yield of a standard sensitizer ($\Phi_{\Delta} = 0.57$ for methylene blue, MB),^{81–83} v_i is the initial rate of DHN consumption, and I and I_{std} are the number of photons absorbed by the sensitizer and the standard, respectively.

$$I = \int I_f(\lambda)(1 - 10^{-\epsilon(\lambda)c_s l}) d\lambda \quad (4)$$

I was estimated from eq 4 using the λ interval 525–535 nm for 3-Pt, 545–555 nm for the 2-Pt-bodipy sensitizers, and 650–660 nm for MB, where $I_f(\lambda)$ is the wavelength dependence of the intensity of the incident light evaluated with a photometer (for values vide supra), $\epsilon(\lambda)$ is the extinction coefficient of the respective sensitizer recorded in CH₂Cl₂/MeOH (9/1), c_s is the concentration of the sensitizer, and l is the length of the cell. Stern–Volmer plots for emission quenching by oxygen or DHN were obtained by admitting appropriate amounts of air or of a DHN stock solution into the cuvette with enough time for equilibration between solvent and gas phase. As for the oxygen quenching experiment, partial pressures were also transformed into concentrations with the literature-known oxygen solubilities in toluene.¹²⁶

Synthesis and Characterization. Except for 8,9-Pt and 3-Pt, all other synthesis followed the representative synthesis protocol provided below. Individual parameters, such as reaction time and temperature, eluent mixtures for chromatography, and crystallization parameters, are given for each compound separately.

Typically, a Young tube was filled with 150 μ mol (1 equiv) of Pt(Et)₂(PEt)₂ and 0.7 mL of C₆D₆. The solution was frozen, evacuated, and heated to 110 °C for 90 min. Inside a glovebox, 1.09 equiv of the respective bodipy dye was added. The mixture was allowed to react for the given time at the stated temperature. Prior to the next step all volatiles were removed, and 1.4 equiv of AgOTf was added. The mixture was refluxed in CH₂Cl₂ for 15 min. The precipitate was filtered off and the resulting solution was added to a methanolic solution of 2 equiv of NaI. After stirring for 20 min the solvents were removed and the crude product was purified as detailed for every compound separately.

trans-Iodo-(1,3,5,7-tetramethyl-8-phenyl-4,4-difluoro-4-bora-3a,4a-diaza-s-indacene-2-yl)-bis(triethylphosphane)platinum(II) (2-Pt-6H). The oxidative addition was performed at 45 °C for 8 h. The final product was purified by column chromatography (silica, CH₂Cl₂/petrol ether 1:2), washed with 4 × 2 mL of *n*-pentane, and dried in vacuo. Yield: 32%. Single crystals for X-ray structure analysis were obtained cooling a saturated C₆H₆/*n*-pentane solution of the complex to –25 °C. ¹H NMR (399.79 MHz, C₆D₆, 304 K): δ 7.07 (m, 3H, H17/H18/H19), 7.00 (m, 2H, H16/H20), 5.75 (s, 1H, H6), 3.02 (s, 3H, H12), 2.70 (s, 3H, H13), 1.72 (m, 12H, P–CH₂CH₃), 1.57 (s with shoulders, 3H, H11), 1.32 (s, 3H, H14), 0.81 (dt, ³J_{HH} = 7.7 Hz, ³J_{PH} = 16.4 Hz, 18H, P–CH₂CH₃). ³¹P NMR (161.84 MHz, C₆D₆, 304 K): δ 9.56 (s with satellites, J_{PP} = 2556 Hz). ¹⁹⁵Pt NMR (85.56 MHz, C₆D₆, 304 K): δ –4784 (t, J_{PP} = 2556 Hz). ¹³C NMR (100.53 MHz, CDCl₃, 300 K): δ 162.3 (s with satellites, ²J_{PC} = 82.8 Hz, C3), 150.0 (s, C5), 143.6 (s with satellites, ³J_{PC} = 45.8 Hz, C10), 139.2 (s, C9), 137.3 (s with shoulders, C8), 136.2 (s, C7), 134.5 (s with satellites, ²J_{PC} = 71.1 Hz, C1), 133.6 (t, ²J_{PC} = 9.4 Hz, C2), 129.6 (s, C15), 129.1 (s, C16/C20), 128.6 (s, C18), 128.4 (s, C17/C19), 119.3 (s, C6), 18.2 (t, ⁴J_{CF} = 2.6 Hz, with satellites ³J_{PC} = 37.2 Hz, C12), 18.1 (s with satellites, ³J_{PC} = 60.2 Hz, C11), 16.0 (vquint, $J_{\text{PC}} = \text{}^3J_{\text{PC}} = 17.9$ Hz, with satellites ²J_{PC} = 36.1 Hz, P–CH₂CH₃), 14.3 (m, C13), 14.1 (s, C14), 8.4 (s with satellites, ³J_{PC} = 24.4 Hz, P–CH₂CH₃). Anal. Calcd for C₃₁H₄₈BF₂IN₂P₂Pt: C, 42.24; H, 5.49; N, 3.18. Found: C, 42.82; H, 5.67; N, 3.39.

trans-Iodo-(6-iodo-1,3,5,7-tetramethyl-8-phenyl-4,4-difluoro-4-bora-3a,4a-diaza-s-indacene-2-yl)-bis(triethylphosphane)platinum(II) (2-Pt-6I). The oxidative addition was conducted at 45 °C for 4 h. The final product was purified by column chromatography (silica, CH₂Cl₂/petrol ether 60:40 → 50:50), the vacuum-dried residue

was washed with 2 mL of *n*-pentane once and dried in vacuo. Yield: 58%. Single crystals were obtained by cooling a saturated C₆H₆/*n*-pentane solution to –25 °C. ¹H NMR (399.79 MHz, C₆D₆, 304 K): δ 7.03 (m, 3H, H17/H18/H19), 6.88 (m, 2H, H16/H20), 3.00 (s, 3H, H12), 2.84 (s, 3H, H13), 1.70 (m, 12 H, P–CH₂CH₃), 1.53 (s with shoulders, 3H, H11), 1.35 (s, 3H, H14), 0.80 (dt, ³J_{HH} = 7.7 Hz, ³J_{PH} = 16.3 Hz, 18H, P–CH₂CH₃). ³¹P NMR (161.84 MHz, C₆D₆, 305 K): δ 9.42 (s with satellites, J_{PP} = 2540 Hz). ¹⁹⁵Pt NMR (85.55 MHz, C₆D₆, 300 K): δ –4779 (t, J_{PP} = 2540 Hz). ¹³C NMR (100.53 MHz, CDCl₃, 300 K): δ 164.8 (s with satellites ²J_{PC} = 85.3 Hz, C3), 149.4 (s, C5), 144.7 (s with satellites ³J_{PC} = 45.8 Hz, C10), 139.1 (s, C8), 136.6 (s, C9), 135.9 (s, C7), 135.4 (t, ²J_{PC} = 9.4 Hz, with satellites $J_{\text{PC}} = 1090$ Hz, C2), 134.9 (s with satellites ²J_{PC} = 37.2 Hz, C1), 129.5 (s, C15), 129.3 (s, C17/C19), 128.9 (s, C18), 128.3 (s, C16/C20), 81.7 (s, C6), 18.4 (t, ⁴J_{CF} = 2.4 Hz, C12), 18.3 (s with satellites ³J_{PC} = 60.9 Hz, C11), 16.2 (s, C14), 16.0 (vquint, $J_{\text{PC}} = \text{}^3J_{\text{PC}} = 17.6$ Hz, with satellites ²J_{PC} = 35.8 Hz, P–CH₂CH₃), 15.5 (t, ⁴J_{CF} = 2.5 Hz, C13), 8.4 (s, with satellites ³J_{PC} = 24.2 Hz, P–CH₂CH₃). Anal. Calcd for C₃₁H₄₇BF₂I₂N₂P₂Pt: C, 36.96; H, 4.70; N, 2.78. Found: C, 36.21, H, 4.34, N, 2.73.

trans-Iodo-(6-iodo-1,3,5,7-tetramethyl-8-mesityl-4,4-difluoro-4-bora-3a,4a-diaza-s-indacene-2-yl)-bis(triethylphosphane)platinum(II) (2-Pt-Mes-6I). Oxidative addition was conducted at 60 °C for 7 h. The final crude product was purified by column chromatography (Al₂O₃, petrol ether/CH₂Cl₂ 6:1). The product fraction was recrystallized from a saturated *n*-pentane/CH₂Cl₂ mixture forming single crystals at –25 °C. Yield: 42%. ¹H NMR (399.78 MHz, CDCl₃, 300 K): δ 6.95 (s, 2H, H17/H19), 2.68 (s, 3H, H12), 2.58 (s, 3H, H13), 2.34 (s, 3H, H22), 2.06 (s, 6H, H21/H23), 1.85 (m, 12H, P–CH₂CH₃), 1.34 (s, 3H, H11), 1.33 (s, 3H, H14), 1.01 (dt, ³J_{HH} = 7.7 Hz, ³J_{PH} = 16.3 Hz, 18H, P–CH₂CH₃). ³¹P NMR (161.83 MHz, CDCl₃, 300 K): δ 5.14 (s with satellites, J_{PP} = 2539 Hz). ¹⁹⁵Pt NMR (85.55 MHz, CDCl₃, 300 K): δ –4802 (t, J_{PP} = 2539 Hz). ¹³C NMR (100.53 MHz, CDCl₃, 300 K): δ 164.1 (s with satellites, ²J_{PC} = 82.1 Hz, C3), 149.4 (s, C5), 144.0 (s with satellites, ³J_{PC} = 43.2 Hz, C10), 138.6 (s, C16/C20), 138.3 (s, C7), 136.2 (s, C9), 134.9 (s, C8), 134.7 (t, ²J_{PC} = 9.7 Hz, C2), 134.2 (s with satellites, ²J_{PC} = 72.1 Hz, C1), 132.0 (s, C15), 129.2 (s, C17/C19), 128.4 (s, C18), 81.3 (s, C6), 21.4 (s, C22), 19.5 (s, C21/C23), 18.4 (t, ⁴J_{CF} = 2.5 Hz, with satellites, ³J_{PC} = 39.5 Hz, C12), 17.3 (s with satellites, ³J_{PC} = 60.5 Hz, C11), 16.2 (vquint, $J_{\text{PC}} = \text{}^3J_{\text{PC}} = 17.5$ Hz, with satellites ²J_{PC} = 35.9 Hz, P–CH₂CH₃), 15.6 (t, ⁴J_{CF} = 2.5 Hz, C13), 15.1 (s, C14), 8.4 (s with satellites, ³J_{PC} = 24.3 Hz, P–CH₂CH₃). Anal. Calcd for C₃₄H₅₃BF₂I₂N₂P₂Pt: C, 38.91; H, 5.09; N, 2.61. Found: C, 39.44; H, 5.22; N, 2.91.

trans-Iodo-(6-ethyl-1,3,5,7-tetramethyl-8-phenyl-4,4-difluoro-4-bora-3a,4a-diaza-s-indacene-2-yl)-bis(triethylphosphane)platinum(II) (2-Pt-6Et). For the oxidative addition step, the reaction mixture was heated to 50 °C for 72 h. The final product was purified on a short silica column (petrol ether/ethyl acetate 40:1). Crystals suitable for X-ray structure analysis were obtained from diffusion of *n*-pentane into a concentrated CH₂Cl₂ solution of the product. Yield 26%. ¹H NMR (399.78 MHz, C₆D₆, 300 K): δ 7.09 (m, 3H, H19/H20/H21), 7.02 (m, 2H, H18/H22), 3.04 (s, 3H, H12), 2.66 (s, 3H, H13), 2.11 (q, ³J_{HH} = 7.5 Hz, 2H, H15), 1.73 (m, 12H, P–CH₂CH₃), 1.59 (s with shoulders, 3H, H11), 1.27 (s, 3H, H14), 0.82 (m, 21 H, H16/P–CH₂CH₃). ³¹P NMR (161.83 MHz, C₆D₆, 300 K): δ 9.75 (s with satellites, J_{PP} = 2561 Hz). ¹⁹⁵Pt NMR (85.55 MHz, C₆D₆, 300 K): δ –4788 (t, J_{PP} = 2561 Hz). ¹³C NMR (100.53 MHz, CDCl₃, 300 K): δ 160.8 (s with satellites, ²J_{PC} = 83 Hz, C3), 149.1 (s, C5), 143.0 (s with satellites, ³J_{PC} = 46 Hz, C10), 137.0 (s, C8), 136.5 (s, C9), 136.3 (s, C7), 134.1 (s with satellites, ²J_{PC} = 71 Hz, C1), 132.7 (t, ²J_{PC} = 9.3 Hz, C2), 131.4 (s, C6), 129.3 (s, C17), 129.1 (s, C19/C21), 128.6 (s, C20), 128.5 (s, C18/C22), 18.16 (m with satellites, ³J_{PC} = 38 Hz, C12), 18.15 (s with satellites, ³J_{PC} = 60 Hz, C11), 17.2 (s, C15), 16.0 (vquint, $J_{\text{PC}} = \text{}^3J_{\text{PC}} = 17.5$ Hz, with satellites ²J_{PC} = 36.1 Hz, P–CH₂CH₃), 15.0 (s, C16), 12.3 (t, ⁴J_{CF} = 2.5 Hz, C13), 11.5 (s, C14), 8.4 (s with satellites, ³J_{PC} = 24.6 Hz, P–CH₂CH₃). Anal. Calcd for C₃₃H₅₂BF₂IN₂P₂Pt: C, 43.58; H, 5.76; N, 3.08. Found: C, 43.50; H, 5.73; N, 3.28.

cis-(8,9- η^2 -3-Chloro-5,7-dimethyl-4,4-difluoro-4-bora-3a,4a-diaza-5-indacene)-bis(triethylphosphane)platinum(II) (**8,9-Pt**). A Young tube was filled with 216 μmol (1 equiv) of $\text{Pt}(\text{Et})_2(\text{PET}_3)_2$ and 0.7 mL of C_6D_6 . The solution was frozen, evacuated, and heated to 110 $^\circ\text{C}$ for 90 min. Inside a glovebox, 1.09 equiv of 3-Cl-bodipy was added. The complex crystallized directly from the reaction mixture forming single crystals. After removing the solvent the compound was dried under reduced pressure. Yield: 94%. The following signal assignment follows the atom numbering in Figure 1. ^1H NMR (399.78 MHz, $\text{THF}-d_6$, 300 K): δ 5.85 (s, 1H, H6), 5.80 (br s, 1H, H1), 5.75 (d, $^3J_{\text{HH}} = 2.54$ Hz, 1H, H2), 3.83 (dd, $^3J_{\text{PH}} = 9.10$ Hz, 4.34 Hz, with satellites $^2J_{\text{PH}} = 49.2$ Hz, 1H, H8), 2.40 (d with shoulders, $^6J_{\text{PH}} = 5.90$ Hz, 3H, H11), 1.82 (m, 3H, H12), 1.80–1.48 (m, 12H, P- CH_2CH_3), 0.96 (m, 18H, P- CH_2CH_3). ^{31}P NMR (161.83 MHz, $\text{THF}-d_6$, 300 K): δ 19.10 (d, $^2J_{\text{PP}} = 9.70$ Hz, with satellites $J_{\text{PP}} = 4801$ Hz, P2), 6.89 (d, $^2J_{\text{PP}} = 9.70$ Hz, with satellites $J_{\text{PP}} = 3321$ Hz, P1). ^{195}Pt (85.51 MHz, $\text{THF}-d_6$, 300 K): δ -4950 (dd, $J_{\text{PP}} = 4801$ Hz, $J_{\text{PtP}} = 3321$ Hz). ^{13}C NMR (150.97 MHz, $\text{THF}-d_6$, 290 K): δ 152.5 (s, C5), 132.8 (s, C10), 127.5 (s, C9), 119.1 (s, C3), 112.8 (s, C6), 106.9 (s, C2), 106.2 (s, C1), 103.3 (s, C7), 42.1 (d, $^2J_{\text{PC}} = 43.6$ Hz, C8), 17.7 (d, $J_{\text{PC}} = 30.7$ Hz, with satellites $^2J_{\text{PC}} = 80.5$ Hz, P2- CH_2CH_3), 15.6 (d with shoulders, $J_{\text{PC}} = 25.7$ Hz, P1- CH_2CH_3), 14.8 (s, C11), 14.3 (s, C12), 8.6 (s with satellites, $^3J_{\text{PC}} = 35.6$ Hz, P2- CH_2CH_3), 8.5 (s with shoulders, P1- CH_2CH_3). Anal. Calcd for $\text{C}_{23}\text{H}_{40}\text{BF}_2\text{ClN}_2\text{P}_2\text{Pt}$: C, 40.28; H, 5.88; N, 4.08. Found: C, 40.47; H, 6.14; N, 4.51.

trans-Iodo-(5,7-dimethyl-4,4-difluoro-4-bora-3a,4a-diaza-5-indacene-3-yl)-bis(triethylphosphane)platinum(II) (**3-Pt**). First, 100 μmol of **8,9-Pt** was loaded into a Young tube and heated in $\text{THF}-d_8$ to 60 $^\circ\text{C}$ for 72 h. The resulting isomeric mixture was treated as explained in the general protocol (vide supra). Purification by column chromatography (silica, ethyl acetate/pentane 10:1) and recrystallization from CH_2Cl_2 yielded orange needles. Yield: 54%. ^1H NMR (399.78 MHz, C_6D_6 , 300 K): δ 6.60 (d with shoulders, $^3J_{\text{HH}} = 4.1$ Hz, 1H, H1), 6.49 (s with satellites, $^3J_{\text{PH}} = 13.3$ Hz, 1H, H8), 6.40 (d, $^3J_{\text{HH}} = 4.1$ Hz, with satellites $^3J_{\text{PH}} = 20.2$ Hz, 1H, H2), 5.72 (s, 1H, H6), 2.57 (s, 3H, H11), 2.11 (m, 6H, P- CH_2CH_3), 1.84 (s, 3H, H12), 1.80 (m, 6H, P- CH_2CH_3), 0.98 (dt, $^3J_{\text{HH}} = 7.9$ Hz, $^3J_{\text{PH}} = 16.3$ Hz, 18H, P- CH_2CH_3). ^{31}P NMR (161.83 MHz, C_6D_6 , 300 K): δ 7.69 (s with satellites, $J_{\text{PP}} = 2547$ Hz). ^{195}Pt (85.55 MHz, C_6D_6 , 300 K): δ -4599 (t, $J_{\text{PP}} = 2547$ Hz). ^{13}C NMR (100.53 MHz, CDCl_3 , 300 K): δ 174.3 (t, $^2J_{\text{PC}} = 10.1$ Hz, with satellites $J_{\text{PC}} = 1150$ Hz, C3), 151.4 (s, C5), 137.7 (s with satellites $^3J_{\text{PC}} = 81.6$ Hz, C10), 136.2 (s, C7), 131.7 (s, C9), 128.7 (s with satellites $^3J_{\text{PC}} = 59.4$ Hz, C1), 128.6 (s with satellites $^2J_{\text{PC}} = 101$ Hz, C2), 117.8 (s, C8), 117.1 (s, C6), 15.7 (vt, $J_{\text{PC}} = ^3J_{\text{PC}} = 17.7$ Hz, with satellites $^2J_{\text{PC}} = 34.8$ Hz, P- CH_2CH_3), 14.7 (s, C11), 11.3 (s, C12), 8.1 (s with satellites, $^3J_{\text{PC}} = 25.5$ Hz, P- CH_2CH_3). Anal. Calcd for $\text{C}_{23}\text{H}_{40}\text{BF}_2\text{IN}_2\text{P}_2\text{Pt}$: C, 35.54; H, 5.19; N, 3.60. Found: C, 35.06; H, 5.26; N, 3.77.

■ ASSOCIATED CONTENT

■ Supporting Information

The Supporting Information is available free of charge on the ACS Publications website at DOI: 10.1021/acs.organomet.7b00806.

^1H , ^{31}P , ^{195}Pt , and ^{13}C NMR spectra; NMR spectroscopic monitoring of the conversion of **8,9-Pt** to **3-Pt**; tabulated data for the X-ray structure determination as well as packing diagrams with intermolecular interactions; electronic absorption spectra; comparison of TD-DFT calculated and experimental spectra; TD-DFT calculations and electron density difference maps; luminescence spectra of **3-Pt** and **8,9-Pt**; comparison of excitation and absorption spectra; spectroscopic monitoring of DHN oxidation to Juglone; cyclic voltammograms; UV/vis/NIR spectroelectrochemistry of **2-Pt-6Et** and 8-mesityl-2,6-diiodo-bodipy; EPR spectrum (PDF)

Spin density distributions and atomic coordinates of the DFT-optimized structures (XYZ)

■ Accession Codes

CCDC 1583615–1583616, 1583637–1583638, 1583640, and 1583642 contain the supplementary crystallographic data for this paper. These data can be obtained free of charge via www.ccdc.cam.ac.uk/data_request/cif, or by emailing data_request@ccdc.cam.ac.uk, or by contacting The Cambridge Crystallographic Data Centre, 12 Union Road, Cambridge CB2 1EZ, UK; fax: +44 1223 336033.

■ AUTHOR INFORMATION

■ Corresponding Author

*E-mail: rainer.winter@uni-konstanz.de.

■ ORCID

Rainer F. Winter: 0000-0001-8381-0647

■ Notes

The authors declare no competing financial interest.

■ ACKNOWLEDGMENTS

Financial support of this work by Deutsche Forschungsgemeinschaft through grant Wi1262/10-2 and the Fachbereich Chemie of the University of Konstanz are gratefully acknowledged. We also thank Bernhard Weibert for data collection and structure refinement in X-ray crystallography as well as Nils Rotthowe and Steffen Oßwald for their help with the EPR spectroscopy.

■ REFERENCES

- (1) Thejo Kalyani, N.; Dhoble, S. J. *Renewable Sustainable Energy Rev.* **2012**, *16*, 2696–2723.
- (2) Ulrich, G.; Ziessel, R.; Harriman, A. *Angew. Chem., Int. Ed.* **2008**, *47*, 1184–1201.
- (3) Kobayashi, H.; Ogawa, M.; Alford, R.; Choyke, P. L.; Urano, Y. *Chem. Rev.* **2010**, *110*, 2620–40.
- (4) Sauer, M.; Heilemann, M. *Chem. Rev.* **2017**, *117*, 7478–7509.
- (5) Pashaei, B.; Shahroosvand, H.; Graetzel, M.; Nazeeruddin, M. K. *Chem. Rev.* **2016**, *116*, 9485–564.
- (6) Ghogare, A. A.; Greer, A. *Chem. Rev.* **2016**, *116*, 9994.
- (7) Skubi, K. L.; Blum, T. R.; Yoon, T. P. *Chem. Rev.* **2016**, *116*, 10035–74.
- (8) Zheng, B.; Sabatini, R. P.; Fu, W. F.; Eum, M. S.; Brennessel, W. W.; Wang, L.; McCamant, D. W.; Eisenberg, R. *Proc. Natl. Acad. Sci. U. S. A.* **2015**, *112*, E3987–96.
- (9) Celli, J. P.; Spring, B. Q.; Rizvi, I.; Evans, C. L.; Samkoe, K. S.; Verma, S.; Pogue, B. W.; Hasan, T. *Chem. Rev.* **2010**, *110*, 2795–838.
- (10) Kamkaew, A.; Lim, S. H.; Lee, H. B.; Kiew, L. V.; Chung, L. Y.; Burgess, K. *Chem. Soc. Rev.* **2013**, *42*, 77–88.
- (11) Dougherty, T. J.; Gomer, C. J.; Henderson, B. W.; Jori, G.; Kessel, D.; Korbek, M.; Moan, J.; Peng, Q. *J. Natl. Cancer Inst.* **1998**, *90*, 889–905.
- (12) Wilson, B. C.; Patterson, M. S. *Phys. Med. Biol.* **2008**, *53*, R61–109.
- (13) Zhao, J.; Ji, S.; Guo, H. *RSC Adv.* **2011**, *1*, 937.
- (14) Singh-Rachford, T. N.; Castellano, F. N. *Coord. Chem. Rev.* **2010**, *254*, 2560–2573.
- (15) Boens, N.; Verbelen, B.; Dehaen, W. *Eur. J. Org. Chem.* **2015**, *2015*, 6577–6595.
- (16) Ulrich, G.; Ziessel, R.; Harriman, A. *Angew. Chem., Int. Ed.* **2008**, *47*, 1184–1201.
- (17) Loudet, A.; Burgess, K. *Chem. Rev.* **2007**, *107*, 4891–4932.
- (18) Zhao, J.; Xu, K.; Yang, W.; Wang, Z.; Zhong, F. *Chem. Soc. Rev.* **2015**, *44*, 8904–8939.
- (19) Harriman, A.; Izzet, G.; Ziessel, R. *J. Am. Chem. Soc.* **2006**, *128*, 10868–10875.

- (20) Zhang, C.; Zhao, J.; Wu, S.; Wang, Z.; Wu, W.; Ma, J.; Guo, S.; Huang, L. *J. Am. Chem. Soc.* **2013**, *135*, 10566–10578.
- (21) Loudet, A.; Burgess, K. *Chem. Rev.* **2007**, *107*, 4891–4932.
- (22) Luo, Y.; Prestwich, G. D. *Bioconjugate Chem.* **1999**, *10*, 755–763.
- (23) Hermanson, G. T. *Bioconjugate techniques*, 3rd ed.; Academic Press: Amsterdam, 2013.
- (24) Niu, S. L.; Massif, C.; Ulrich, G.; Renard, P. Y.; Romieu, A.; Ziessel, R. *Chem. - Eur. J.* **2012**, *18*, 7229–42.
- (25) Yogo, T.; Urano, Y.; Ishitsuka, Y.; Maniwa, F.; Nagano, T. *J. Am. Chem. Soc.* **2005**, *127*, 12162–12163.
- (26) Epelde-Elezcano, N.; Palao, E.; Manzano, H.; Prieto-Castaneda, A.; Agarrabaitia, A. R.; Tabero, A.; Villanueva, A.; de la Moya, S.; Lopez-Arbeloa, I.; Martinez-Martinez, V.; Ortiz, M. J. *Chem. - Eur. J.* **2017**, *23*, 4837–4848.
- (27) Ventura, B.; Marconi, G.; Bröring, M.; Krüger, R.; Flamigni, L. *New J. Chem.* **2009**, *33*, 428–438.
- (28) Cakmak, Y.; Kolemen, S.; Duman, S.; Dede, Y.; Dolen, Y.; Kilic, B.; Kostereli, Z.; Yildirim, L. T.; Dogan, A. L.; Guc, D.; Akkaya, E. U. *Angew. Chem., Int. Ed.* **2011**, *50*, 11937–41.
- (29) Duman, S.; Cakmak, Y.; Kolemen, S.; Akkaya, E. U.; Dede, Y. *J. Org. Chem.* **2012**, *77*, 4516–27.
- (30) Wu, W.; Cui, X.; Zhao, J. *Chem. Commun. (Cambridge, U. K.)* **2013**, *49*, 9009–11.
- (31) Zhao, J.; Xu, K.; Yang, W.; Wang, Z.; Zhong, F. *Chem. Soc. Rev.* **2015**, *44*, 8904–8939.
- (32) Wu, W.; Zhao, J.; Sun, J.; Huang, L.; Yi, X. *J. Mater. Chem. C* **2013**, *1*, 705–716.
- (33) Jia, H.; Küçüköz, B.; Xing, Y.; Majumdar, P.; Zhang, C.; Karatay, A.; Yaglioglu, G.; Elmali, A.; Zhao, J.; Hayvali, M. *J. Mater. Chem. C* **2014**, *2*, 9720–9736.
- (34) Yang, W.; Karatay, A.; Zhao, J.; Song, J.; Zhao, L.; Xing, Y.; Zhang, C.; He, C.; Yaglioglu, H. G.; Hayvali, M.; Elmali, A.; Kucukoz, B. *Inorg. Chem.* **2015**, *54*, 7492–505.
- (35) Majumdar, P.; Cui, X.; Xu, K.; Zhao, J. *Dalton Trans.* **2015**, *44*, 4032–45.
- (36) Galletta, M.; Campagna, S.; Quesada, M.; Ulrich, G.; Ziessel, R. *Chem. Commun. (Cambridge, U. K.)* **2005**, 4222–4.
- (37) Rachford, A. A.; Ziessel, R.; Bura, T.; Retailleau, P.; Castellano, F. N. *Inorg. Chem.* **2010**, *49*, 3730–6.
- (38) Wu, W.; Sun, J.; Cui, X.; Zhao, J. *J. Mater. Chem. C* **2013**, *1*, 4577.
- (39) Yi, X.; Zhao, J.; Sun, J.; Guo, S.; Zhang, H. *Dalton Trans.* **2013**, *42*, 2062–74.
- (40) Wang, P.; Koo, Y. H.; Kim, W.; Yang, W.; Cui, X.; Ji, W.; Zhao, J.; Kim, D. *J. Phys. Chem. C* **2017**, *121*, 11117–11128.
- (41) Zhong, F.; Karatay, A.; Zhao, L.; Zhao, J.; He, C.; Zhang, C.; Yaglioglu, H. G.; Elmali, A.; Kucukoz, B.; Hayvali, M. *Inorg. Chem.* **2015**, *54*, 7803–17.
- (42) Hsu, C.-W.; Lin, C.-C.; Chung, M.-W.; Chi, Y.; Lee, G.-H.; Chou, P.-T.; Chang, C.-H.; Chen, P.-Y. *J. Am. Chem. Soc.* **2011**, *133*, 12085–12099.
- (43) Yu-Tzu Li, E.; Jiang, T. Y.; Chi, Y.; Chou, P. T. *Phys. Chem. Chem. Phys.* **2014**, *16*, 26184–92.
- (44) Chang, Y.-C.; Tang, K.-C.; Pan, H.-A.; Liu, S.-H.; Koshevoy, I. O.; Karttunen, A. J.; Hung, W.-Y.; Cheng, M.-H.; Chou, P.-T. *J. Phys. Chem. C* **2013**, *117*, 9623–9632.
- (45) Wang, B.-Y.; Karikachery, A. R.; Li, Y.; Singh, A.; Lee, H. B.; Sun, W.; Sharp, P. R. *J. Am. Chem. Soc.* **2009**, *131*, 3150–3151.
- (46) Lentijo, S.; Miguel, J. A.; Espinet, P. *Inorg. Chem.* **2010**, *49*, 9169–77.
- (47) Lee, H. B.; Sharp, P. R. *Organometallics* **2005**, *24*, 4875–4877.
- (48) Choi, H.; Kim, C.; Park, K.-M.; Kim, J.; Kang, Y.; Ko, J. *J. Organomet. Chem.* **2009**, *694*, 3529–3532.
- (49) Singh, A.; Sharp, P. R. *J. Am. Chem. Soc.* **2006**, *128*, 5998–5999.
- (50) Vu, T. T.; Badré, S.; Dumas-Verdes, C. c.; Vachon, J.-J.; Julien, C.; Audebert, P.; Senotrusova, E. Y.; Schmidt, E. Y.; Trofimov, B. A.; Pansu, R. B.; Clavier, G.; Méallet-Renault, R. *J. Phys. Chem. C* **2009**, *113*, 11844–11855.
- (51) Wu, W.; Guo, H.; Wu, W.; Ji, S.; Zhao, J. *J. Org. Chem.* **2011**, *76*, 7056–64.
- (52) Lim, H.; Seo, S.; Pascal, S.; Bellier, Q.; Rigaut, S.; Park, C.; Shin, H.; Maury, O.; Andraud, C.; Kim, E. *Sci. Rep.* **2016**, *6*, 18867.
- (53) Nepomnyashchii, A. B.; Bröring, M.; Ahrens, J.; Bard, A. J. *J. Am. Chem. Soc.* **2011**, *133*, 8633–8645.
- (54) Huang, L.; Yang, W.; Zhao, J. *J. Org. Chem.* **2014**, *79*, 10240–10255.
- (55) Lazarides, T.; McCormick, T. M.; Wilson, K. C.; Lee, S.; McCamant, D. W.; Eisenberg, R. *J. Am. Chem. Soc.* **2011**, *133*, 350–64.
- (56) Goze, C.; Ulrich, G.; Mallon, L. J.; Allen, B. D.; Harriman, A.; Ziessel, R. *J. Am. Chem. Soc.* **2006**, *128*, 10231–10239.
- (57) McCarthy, T. J.; Nuzzo, R. G.; Whitesides, G. M. *J. Am. Chem. Soc.* **1981**, *103*, 3396–3403.
- (58) Strawser, D.; Karton, A.; Zenkina, O. V.; Iron, M. A.; Shimon, L. J.; Martin, J. M.; van der Boom, M. E. *J. Am. Chem. Soc.* **2005**, *127*, 9322–3.
- (59) Irmeler, P.; Winter, R. F. *Dalton Trans.* **2016**, *45*, 10420–10434.
- (60) Bauer, F.; Braunschweig, H.; Gruss, K.; Kupfer, T. *Organometallics* **2011**, *30*, 2869–2884.
- (61) Braunschweig, H.; Bertermann, R.; Brenner, P.; Burzler, M.; Dewhurst, R. D.; Radacki, K.; Seeler, F. *Chem. - Eur. J.* **2011**, *17*, 11828–37.
- (62) Farrugia, L. J. *J. Appl. Crystallogr.* **2012**, *45*, 849–854.
- (63) Geist, F.; Jackel, A.; Winter, R. F. *Inorg. Chem.* **2015**, *54*, 10946–10957.
- (64) Al Anshori, J.; Slanina, T.; Palao, E.; Klán, P. *Photochem. Photobiol. Sci.* **2016**, *15*, 250–9.
- (65) Geist, F.; Jackel, A.; Irmeler, P.; Linseis, M.; Malzkuhn, S.; Kuss-Petermann, M.; Wenger, O. S.; Winter, R. F. *Inorg. Chem.* **2017**, *56*, 914.
- (66) Whited, M. T.; Djurovich, P. I.; Roberts, S. T.; Durrell, A. C.; Schlenker, C. W.; Bradforth, S. E.; Thompson, M. E. *J. Am. Chem. Soc.* **2011**, *133*, 88–96.
- (67) Wu, W.; Zhao, J.; Guo, H.; Sun, J.; Ji, S.; Wang, Z. *Chem. - Eur. J.* **2012**, *18*, 1961–1968.
- (68) Siebrand, W.; Williams, D. F. *J. Chem. Phys.* **1968**, *49*, 1860–1871.
- (69) Englman, R.; Jortner, J. *Mol. Phys.* **1970**, *18*, 145–164.
- (70) Scott, D. R.; Maltenieks, O. J. *Phys. Chem.* **1968**, *72*, 3354–3356.
- (71) Zaitsev, A. B.; Méallet-Renault, R.; Schmidt, E. Y.; Mikhaleva, A. b. I.; Badré, S.; Dumas, C.; Vasil'tsov, A. M.; Zorina, N. V.; Pansu, R. B. *Tetrahedron* **2005**, *61*, 2683–2688.
- (72) Badré, S.; Monnier, V.; Méallet-Renault, R.; Dumas-Verdes, C.; Schmidt, E. Y.; Mikhaleva, A. b. I.; Laurent, G.; Levi, G.; Ibanez, A.; Trofimov, B. A.; Pansu, R. B. *J. Photochem. Photobiol., A* **2006**, *183*, 238–246.
- (73) Irmeler, P.; Winter, R. F. *Dalton Trans.* **2016**, *45*, 10420–34.
- (74) Yang, P.; Zhao, J.; Wu, W.; Yu, X.; Liu, Y. *J. Org. Chem.* **2012**, *77*, 6166–78.
- (75) Huang, L.; Zhao, J. *RSC Adv.* **2013**, *3*, 23377–23388.
- (76) Huang, L.; Zhao, J.; Guo, S.; Zhang, C.; Ma, J. *J. Org. Chem.* **2013**, *78*, 5627–5637.
- (77) Wu, W.; Geng, Y.; Fan, W.; Li, Z.; Zhan, L.; Wu, X.; Zheng, J.; Zhao, J.; Wu, M. *RSC Adv.* **2014**, *4*, 51349–51352.
- (78) Gorman, A.; Killoran, J.; O'Shea, C.; Kenna, T.; Gallagher, W. M.; O'Shea, D. F. *J. Am. Chem. Soc.* **2004**, *126*, 10619–31.
- (79) Awuah, S. G.; You, Y. *RSC Adv.* **2012**, *2*, 11169–11183.
- (80) Rehm, D.; Weller, A. *Isr. J. Chem.* **1970**, *8*, 259–271.
- (81) Usui, Y. *Chem. Lett.* **1973**, *2*, 743–744.
- (82) Wilkinson, F.; Helman, W. P.; Ross, A. B. *J. Phys. Chem. Ref. Data* **1993**, *22*, 113–262.
- (83) Chaon, J. N.; Jamieson, G. R.; Sinclair, R. S. *Chem. Phys. Lipids* **1987**, *43*, 81–99.
- (84) Rurack, K.; Kollmannsberger, M.; Daub, J. *Angew. Chem., Int. Ed.* **2001**, *40*, 385–387.
- (85) Hattori, S.; Ohkubo, K.; Urano, Y.; Sunahara, H.; Nagano, T.; Wada, Y.; Tkachenko, N. V.; Lemmetyinen, H.; Fukuzumi, S. *J. Phys. Chem. B* **2005**, *109*, 15368–75.

- (86) Teki, Y.; Tamekuni, H.; Haruta, K.; Takeuchi, J.; Miura, Y. *J. Mater. Chem.* **2008**, *18*, 381–391.
- (87) Summers, G. H.; Lefebvre, J. F.; Black, F. A.; Davies, E. S.; Gibson, E. A.; Pullerits, T.; Wood, C. J.; Zidek, K. *Phys. Chem. Chem. Phys.* **2016**, *18*, 1059–70.
- (88) Hendel, S. J.; Poe, A. M.; Khomein, P.; Bae, Y.; Thayumanavan, S.; Young, E. R. *J. Phys. Chem. A* **2016**, *120*, 8794–8803.
- (89) Iagatti, A.; Cupellini, L.; Biagiotti, G.; Caprasecca, S.; Fedeli, S.; Lapini, A.; Ussano, E.; Cicchi, S.; Foggi, P.; Marcaccio, M.; Mennucci, B.; Di Donato, M. *J. Phys. Chem. C* **2016**, *120*, 16526–16536.
- (90) Jin, G. F.; Cho, Y. J.; Wee, K. R.; Hong, S. A.; Suh, I. H.; Son, H. J.; Lee, J. D.; Han, W. S.; Cho, D. W.; Kang, S. O. *Dalton Trans.* **2015**, *44*, 2780–7.
- (91) Richards, V. J.; Gower, A. L.; Smith, J. E.; Davies, E. S.; Lahaye, D.; Slater, A. G.; Lewis, W.; Blake, A. J.; Champness, N. R.; Kays, D. L. *Chem. Commun. (Cambridge, U. K.)* **2012**, *48*, 1751–3.
- (92) Hendel, S. J.; Poe, A. M.; Khomein, P.; Bae, Y.; Thayumanavan, S.; Young, E. R. *J. Phys. Chem. A* **2016**, *120*, 8794–8803.
- (93) Belzile, M.-N.; Godin, R.; Durantini, A. M.; Cosa, G. *J. Am. Chem. Soc.* **2016**, *138*, 16388–16397.
- (94) Ruff, A.; Heyer, E.; Roland, T.; Haacke, S.; Ziessel, R.; Ludwigs, S. *Electrochim. Acta* **2015**, *173*, 847–859.
- (95) Benniston, A. C.; Copley, G.; Harriman, A.; Howgego, D.; Harrington, R. W.; Clegg, W. *J. Org. Chem.* **2010**, *75*, 2018–27.
- (96) Krejčík, M.; Daněš, M.; Hartl, F. J. *Electroanal. Chem. Interfacial Electrochem.* **1991**, *317*, 179–187.
- (97) Chen, Y.; Zhao, J.; Guo, H.; Xie, L. *J. Org. Chem.* **2012**, *77*, 2192–206.
- (98) Fu, L.; Jiang, F. L.; Fortin, D.; Harvey, P. D.; Liu, Y. *Chem. Commun. (Cambridge, U. K.)* **2011**, *47*, 5503–5.
- (99) Lerrick, R. I.; Winstanley, T. P.; Haggerty, K.; Wills, C.; Clegg, W.; Harrington, R. W.; Bultinck, P.; Herrebout, W.; Benniston, A. C.; Hall, M. J. *Chem. Commun. (Cambridge, U. K.)* **2014**, *50*, 4714–6.
- (100) Ghelfi, M.; Ulatowski, L.; Manor, D.; Atkinson, J. *Bioorg. Med. Chem.* **2016**, *24*, 2754–61.
- (101) Zhou, X.; Yu, C.; Feng, Z.; Yu, Y.; Wang, J.; Hao, E.; Wei, Y.; Mu, X.; Jiao, L. *Org. Lett.* **2015**, *17*, 4632–5.
- (102) Herrendorf, W.; Bärnighausen, W. *HABITUS, program for the optimization of the crystal shape for numerical absorption correction in X-SHAPE*, version 1.06; Fa. Stoe: Darmstadt, Germany, 1999.
- (103) Sheldrick, G. M. *SHELXL-97, Program for Crystal Structure Solution and Refinement*; Universität Göttingen: Göttingen, Germany, 1997.
- (104) Sheldrick, G. M. *Acta Crystallogr., Sect. A: Crystallogr.* **2008**, *64*, 112–122.
- (105) Sheldrick, G. M. *Acta Crystallogr., Sect. A: Crystallogr.* **2008**, *64*, 112–22.
- (106) Dolomanov, O. V.; Bourhis, L. J.; Gildea, R. J.; Howard, J. A. K.; Puschmann, H. *J. Appl. Crystallogr.* **2009**, *42*, 339–341.
- (107) Spek, A. L. *Acta Crystallogr., Sect. D: Biol. Crystallogr.* **2009**, *65*, 148–155.
- (108) Macrae, C. F.; Bruno, I. J.; Chisholm, J. A.; Edgington, P. R.; McCabe, P.; Pidcock, E.; Rodriguez-Monge, L.; Taylor, R.; Van De Streek, J.; Wood, P. A. *J. Appl. Crystallogr.* **2008**, *41*, 466–470.
- (109) Stoll, S.; Schweiger, A. *J. Magn. Reson.* **2006**, *178*, 42–55.
- (110) Frisch, M. J.; Trucks, G. W.; Schlegel, H. B.; Scuseria, G. E.; Robb, M. A.; Cheeseman, J. R.; Scalmani, G.; Barone, V.; Mennucci, B.; Petersson, G. A.; Nakatsuji, H.; Caricato, M.; Li, X.; Hratchian, H. P.; Izmaylov, A. F.; Bloino, J.; Zheng, G.; Sonnenberg, J. L.; Hada, M.; Ehara, M.; Toyota, K.; Fukuda, R.; Hasegawa, J.; Ishida, M.; Nakajima, T.; Honda, Y.; Kitao, O.; Nakai, H.; Vreven, T.; Montgomery, J. A., Jr.; Peralta, J. E.; Ogliaro, F.; Bearpark, M.; Heyd, J. J.; Brothers, E.; Kudin, K. N.; Staroverov, V. N.; Kobayashi, R.; Normand, J.; Raghavachari, K.; Rendell, A.; Burant, J. C.; Iyengar, S. S.; Tomasi, J.; Cossi, M.; Rega, N.; Millam, J. M.; Klene, M.; Knox, J. E.; Cross, J. B.; Bakken, V.; Adamo, C.; Jaramillo, J.; Gomperts, R.; Stratmann, R. E.; Yazyev, O.; Austin, A. J.; Cammi, R.; Pomelli, C.; Ochterski, J. W.; Martin, R. L.; Morokuma, K.; Zakrzewski, V. G.; Voth, G. A.; Salvador, P.; Dannenberg, J. J.; Dapprich, S.; Daniels, A. D.; Farkas, O.; Foresman, J. B.; Ortiz, J. V.; Cioslowski, J.; Fox, D. J. *Gaussian 09*, revision E.01; Gaussian, Inc.: Wallingford, CT, 2009.
- (111) Gunnarsson, O.; Lundqvist, B. I. *Phys. Rev. B* **1976**, *13*, 4274–4298.
- (112) Küchle, W.; Dolg, M.; Stoll, H.; Preuss, H. *J. Chem. Phys.* **1994**, *100*, 7535–7542.
- (113) Dolg, M.; Stoll, H.; Preuss, H. *J. Chem. Phys.* **1989**, *90*, 1730.
- (114) Andrae, D.; Häußermann, U.; Dolg, M.; Stoll, H.; Preuß, H. *Theor. Chim. Acta* **1990**, *77*, 123–141.
- (115) Hariharan, P. C.; Pople, J. A. *Theor. Chim. Acta* **1973**, *28*, 213–222.
- (116) Perdew, J. P.; Burke, K.; Ernzerhof, M. *Phys. Rev. Lett.* **1996**, *77*, 3865–3868.
- (117) Adamo, C.; Barone, V. *J. Chem. Phys.* **1999**, *110*, 6158–6170.
- (118) Cancés, E.; Mennucci, B.; Tomasi, J. *J. Chem. Phys.* **1997**, *107*, 3032–3041.
- (119) Mennucci, B.; Tomasi, J. *J. Chem. Phys.* **1997**, *106*, 5151–5158.
- (120) Cossi, M.; Rega, N.; Scalmani, G.; Barone, V. *J. Comput. Chem.* **2003**, *24*, 669–681.
- (121) Scalmani, G.; Frisch, M. J. *J. Chem. Phys.* **2010**, *132*, 114110.
- (122) Runge, E.; Gross, E. K. U. *Phys. Rev. Lett.* **1984**, *52*, 997–1000.
- (123) O’Boyle, N. M.; Tenderholt, A. L.; Langner, K. M. *J. Comput. Chem.* **2008**, *29*, 839–845.
- (124) Takizawa, S.-y.; Aboshi, R.; Murata, S. *Photochem. Photobiol. Sci.* **2011**, *10*, 895–903.
- (125) Adarsh, N.; Shanmugasundaram, M.; Avirah, R. R.; Ramaiah, D. *Chem. - Eur. J.* **2012**, *18*, 12655–12662.
- (126) Field, L. R.; Wilhelm, E.; Battino, R. *J. Chem. Thermodyn.* **1974**, *6*, 237–243.